# Long Term Assimilation of Directional Wave Data From CFOSAT in the Wave Prediction Model MFWAM

Emma Bedossa, Lotfi Aouf, Danièle Hauser, Hervé Giordani, Fabrice Collard

AGU ADVANCING EARTH AND SPACE SCIENCES

Earth and Space Science

RESEARCH ARTICLE
10.1029/2025EA004743

# Long Term Assimilation of Directional Wave Data From CFOSAT in the Wave Prediction Model MFWAM

**E. Bedossa[1,2], L. Aouf[1], D. Hauser[3], A. Dalphinet[1], H. Giordani[1], and F. Collard[4]**

[1]Météo-France, CNRS, University Toulouse, CNRM, Toulouse, France, [2]CNES, Toulouse, France, [3]LATMOS/IPSL, Guyancourt, France, [4]OceanDataLab, Brest, France

**Key Points:**

- Assimilating SWIM wave height and wavenumbers components reduces wave heights bias and scatter index in the Southern Ocean of 40% and 18%
- Assimilating wave heights alone degrades the peak period bias, highlighting the importance of assimilation of SWIM spectral observations
- Assimilation of SWIM wave heights and wavenumbers components improves forecasts beyond 4 days, especially in energetic swell-dominant areas

**Correspondence to:**
L. Aouf,
lotfi.aouf@meteo.fr

**Citation:**
Bedossa, E., Aouf, L., Hauser, D., Dalphinet, A., Giordani, H., & Collard, F. (2026). Long term assimilation of directional wave data from CFOSAT in the wave prediction model MFWAM. *Earth and Space Science*, *13*, e2025EA004743. https://doi.org/10.1029/2025EA004743

Received 8 SEP 2025
Accepted 25 MAR 2026

**Author Contributions:**
**Conceptualization:** E. Bedossa, L. Aouf
**Data curation:** F. Collard
**Formal analysis:** E. Bedossa, L. Aouf, D. Hauser
**Investigation:** E. Bedossa, L. Aouf, D. Hauser, A. Dalphinet
**Methodology:** E. Bedossa, L. Aouf
**Supervision:** L. Aouf, D. Hauser, A. Dalphinet, H. Giordani, F. Collard
**Validation:** L. Aouf
**Visualization:** E. Bedossa, A. Dalphinet
**Writing – original draft:** E. Bedossa
**Writing – review & editing:** E. Bedossa, L. Aouf, D. Hauser, A. Dalphinet, H. Giordani, F. Collard



**Abstract** Recently, satellite wave observations have stepped forward with the innovative measurements from the wave scatterometer SWIM of the CFOSAT mission which provides both the significant wave height (SWH) along-track at nadir look and the directional wave spectra on off-nadir incidence angle. This work aims at evaluating the impact of the assimilation of SWIM wave observations on the wave forecast, and at analyzing the improvement of estimating wave properties. Runs of the MFWAM model with and without assimilation of SWIM data have been performed for a long period from 2019 to 2022. SWIM wave data is used with the improved level 2 processing version 6, operational since June 2023. The validation of model runs is performed against independent SWH from independent altimeters and against drifting wave buoys parameters provided by the SOFAR network during the year 2021. The results show an improvement of integrated wave parameters induced by the assimilation compared with observations, especially when wavenumbers and SWH are assimilated jointly. The scatter index of SWH when assimilation of wave heights from SWIM is activated is improved by 15%, globally and 9.5% in the tropics. This impact increases to 18% for the Southern ocean, known for severe storms and long swell dominant sea state. In this study we also show that the assimilation of directional wave spectra is more efficient to reduce the bias and scatter index on the peak period, than the assimilation of significant wave height only, and we discuss the improvement of the assimilation scheme in the MFWAM model.

**Plain Language Summary** The CFOSAT (Chinese-French Oceanic SATellite) satellite mission, launched on 29 October 2018, provides directional wave spectra thanks to the SWIM wave scatterometer. These directional observations give a detailed representation of wind sea and swell, which are relevant for operational wave forecasting and ocean/wave/atmosphere coupling. Innovative wave observations from satellites are needed in order to improve wave physics and preparedness to extreme conditions. This work presents an assessment on the impact of assimilating SWIM wave data in the wave model MFWAM. The analysis shows the importance of accounting for wavelength and wave direction observations at different stages of wave evolution from wind sea to swell regimes. Indeed assimilation of such observations improves peak periods and significant wave heights, particularly in ocean regions where strong uncertainties on the wind forcing remain, such as the Southern Ocean. The assimilation of SWIM wave data opens interesting perspectives to better model wave growth and propagation in global ocean and in critical seas such as the Southern Ocean.

## 1. Introduction

Ocean waves forecasting is crucial for predicting and analyzing the exchanges of momentum and heat fluxes at the atmosphere/ocean interface (Shimura & Nobuhito, 2019) and for the protection against natural hazards in coastal regions during severe storms. Since the availability of wave observations from satellites, the assimilation of observations in operational wave models has been mainly based on the significant wave heights from altimetry. It has induced a significant improvement of the prediction of integrated sea-state parameters and reduced uncertainties related to wind forcing from Numerical Weather Prediction (NWP) models (Smit et al., 2021; Yu et al., 2018). However, the assimilation of SWH (Significant Wave Height) has a limited impact over the forecast period, as indicated by Saulter et al. (2020). The wave models still present uncertainties in the source terms of wind-wave growth and dissipation by deep-water wave breaking. Despite improvements in the physics of these source terms following the work of Ardhuin et al. (2010), Zieger et al. (2015), Babanin et al. (2014), Alday & Ardhuin (2023), Janssen & Bidlot (2023), and Janssen et al. (2014), there is still room for improvement by using satellite wave observations such as the one provided by CFOSAT and Sentinel-1 missions, and also the availability of wave data from drifting buoys (Smit et al., 2021 (SOFAR buoys), Thomson et al., 2021 (SWIFT

measurements) and Rabault et al., 2021 (OpenMetBuoy)). The development of assimilation schemes capable of jointly using SWH and directional wave spectra is a major asset in understanding and better constraining the wave model physics. First tests carried out by Aouf et al. (2006, 2019), show that it has an impact that remains effective longer into the forecast period (more than 3 days-forecast) than when assimilating only SWH. The observations provided by the SWIM instrument of the CFOSAT satellite can contribute to this evolution. Recent examples include the improved transition from wind waves to swell after assimilation of wavenumber components of CFOSAT/SWIM-observed partitions under unlimited fetch conditions in the Southern Ocean (Aouf et al., 2021). Work on the assimilation of buoy wave spectra with good data coverage from SOFAR buoys network has also shown a significant impact on integrated sea state parameters (Houghton et al., 2022). However critical ocean areas such as near the marginal ice zone and closed seas are still under-represented by buoys.

This work aims first to assess the impact of assimilating SWIM directional wave spectra and significant wave height on the analysis fields from the MFWAM model over a long period, namely over 4 years from 2019 to 2022. We analyze the impact of the assimilation on both the significant wave height and the peak period of the waves, and not only at the global scale but also in specific oceanic basins, some of them being critical because of the high wave conditions or specific fetch conditions. Secondly, this work aims to assess the impact of assimilating SWIM directional wave spectra and significant wave height on forecast fields from the MFWAM model. The paper is organized as follows. Following this introduction, Section 2 describes the main configurations of the wave model and the wave data used for assimilation and validation. Section 3 first presents the control run and the analysis increment due to the assimilation on wave parameters, and then compares the analysis fields from the MFWAM model results obtained with different versions of data assimilation, against independent satellite altimeter and buoy wave observations. Section 4 discusses the impact of SWIM data assimilation on MFWAM forecasts over time during a forecast period of several days, and finally, Section 5 discusses limitations of the assimilation scheme we found in this work, and finally it summarizes the main finding and the conclusions of this study.

## 2. Material and Methods

### 2.1. Wave Model Description

The wave model used is based on a global configuration of the MFWAM model with a grid resolution of 25 km and spectral resolution of 24 directions and 30 frequencies, and 3-hourly outputs. The minimum wave frequency is 0.035 Hz and a geometrical increase of 1.1 is applied for the following frequencies. MFWAM is the French version of the WAM model developed at ECMWF (see ECWAM documentation). The wave physics of the MFWAM model is the same as the one currently used operationally for the Copernicus Marine Service (QUID available here https://doi.org/10.48670/moi-00017). The model uses source terms for wind wave generation and dissipation by breaking in deep water based on the ST4 physics developed in Ardhuin et al. (2010). The model accounts for nonlinear wave-wave interactions source term approximated by the Discrete Interactions Approximation (DIA) scheme (Hasselmann & Hasselmann, 1985). Unlike ECWAM, this model version does not include online coupling between waves and wind. Note also that the model does not include a wave-ice interaction term and does not account for wave-current interaction. The model is driven by 3-hourly 10-m height winds provided by the analysis from the IFS atmospheric system of ECMWF. The ice fraction is also prescribed from IFS. Several model experiments have been implemented in this work for the period 2019–2022. CNT stands for the control run without assimilation, HS_ASSIM stands for MFWAM model run with assimilation of only SWIM-nadir observations and SPEC_ASSIM stands for MFWAM model run with assimilation of only wavenumbers components of partitions derived from SWIM. Finally, SPEC_HS_ASSIM performs the MFWAM model run with assimilation of both the SWH from SWIM-nadir observations and of the wavenumber components of partitions derived from the SWIM directional wave spectra. In this latter case (SPEC_HS_ASSIM), assimilation of significant wave height and wave number components are carried out sequentially.

### 2.2. SWIM Wave Observations Used in Assimilation

The wave data that are assimilated in this study come from the SWIM radar observations. We precise that no other data from any instruments other than SWIM are assimilated in the experiments used in this paper. SWIM is a Ku-Band radar instrument carried by the China France Oceanography Satellite (CFOSAT) - see Hauser et al., 2017- which was launched in October 2018. SWIM operates with a multi-incidence configuration, which includes a nadir viewing beam like in standard altimeter missions and 5 off-nadir beams pointing the surface at about 2°, 4°,

6°, 8° and 10° from nadir. All the beams scan over 360° in azimuth. The three outer beams (pointing at 6°, 8°, and 10°) were designed to measure the directional wave spectra according to the principle described in Hauser et al. (2017). The revisit cycle of CFOSAT is 13 days. Shortly after the satellite launch, the observations were validated based on a preliminary processing version (Hauser et al., 2021). Since then, several corrections have been applied. Firstly, to correct for the speckle noise perturbation and the normalization. Secondly, to normalize the energy of the directional wave spectra from the off-nadir beams by using the SWH nadir beam information. In this study we focus on using wave data from the processing version 6.0.1 which is the most up to date version spanning the longest period.

Here we use the SWH derived from the nadir beam observation, and the wave spectra, obtained from the beam 10°. It has been shown in several previous studies (Hauser et al., 2021) that the wave spectra retrieved from this 10° beam are of better quality compared to those from the 6° and 8° beams. The wave spectra are provided as wave slope spectra defined over 32 wavenumber bins (increments increasing exponentially from 4.60 $10^{-4}$ to 0.277 rad/m) and 24 directions (every 15° from 0 to 360° with an imposed 180° symmetry). Before searching for wave partitions as described in Section 2.3, the SWIM wave slope spectra ($E(k,\theta)$) are converted into height spectra ($E(f,\theta)$) and expressed in terms of frequency by using the following relationship:

$$E(f,\theta) = 4\pi\sqrt{\frac{k}{g}}E(k,\theta) \tag{1}$$

where $k$ is the wavenumber, $f$ the frequency and $g$ the gravitational constant.

### 2.3. Assimilation Scheme

The assimilation system used in the MFWAM model is composed of two parts that independently assimilate significant wave heights provided by the nadir observations and parameters of the directional wave spectra provided from the SWIM beam pointing at 10° from the nadir. For both types of data, the assimilation time step is 3 hr. For each 3-hr time step, the amount of information from SWIM to be assimilated into MFWAM is roughly around 2,500 spectra and 1,600 SWH at the global level.

The first part is the assimilation of SWH, which consists of applying an optimal interpolation between model and observation data, and of spreading the corrections according to a correlation model that follows an exponential decay. This latter depends on the distance of influence of the observations and the correlation length, as indicated in Aouf and Lefèvre (2015). For SWH assimilation, the correlation length is estimated at 300 km and remains constant over the entire domain. The ratio of observation error to model error is considered equal to 1. The assimilation of SWH includes a rescaling of the wave spectrum energy in order to apply the correction separately on the wind-wave and swell parts. The principle of this scheme is the following: assimilation of wave height data from SWIM nadir using optimal interpolation yields an analyzed wave height field, denoted $H_s^a$. At each model grid point, the energy of the directional wave spectrum $E^a(f,\theta)$ corresponding to $H_s^a$ is then redistributed using the approach of Lionello et al. (1992) applied on the first-guess directional wave height spectrum $E_b$. This is carried out by relating $E^a$ and $E^b$ as follows:

$$E^a(f,\theta) = \mathrm{A}E^b(Bf,\theta) \tag{2}$$

This expression includes parameters $A$ and $B$, which are used to reshape the analyzed spectrum. This implies that assimilating $H_s$ alone also affects the spectral shape, particularly because of the coefficient $B$. The parameterization of $A$ and $B$ depend on the dominant wave regime of the spectrum, either wind-sea or swell.

In the MFWAM assimilation scheme, two-dimensional wave spectra are analyzed to separate wind sea from swell: if the wind sea energy is larger than 3/4 times the total energy, the wave regime is considered as windsea. If this condition is not satisfied, the regime is considered as swell.

Lionello et al. (1992) showed that in the wind-sea regime conditions, the parameters $A$ and $B$ of Equation 2 are explicitly related to the duration-limited wave growth equations, in line with Equations (11) and (12) from Toledano et al. (2022). In consequence, $A$ and $B$ can be expressed as:

$$A = \left(\frac{H_s^a}{H_s^b}\right)^2 B \text{ and } B = \frac{f_m^b}{f_m^a} \tag{3}$$

where $f_m^a$ and $f_m^b$ are the mean frequencies of the analyzed spectrum and of the first-guess spectrum, respectively, and $H_s^a$ and $H_s^b$ the analyzed and first-guess significant wave height, respectively

In swell conditions, the growth equations for waves under the action of wind do not apply. Instead, the assumption is that the swell steepness is conserved when the significant is modified by assimilation (Lionello & Janssen, 1990; Lionello et al., 1992). The steepness is expressed as $s = k_m H_s/8\pi$ (Lionello and Janssen (1990)). The authors of this study also assumed that the effective decay time and therefore the wave steepness is not affected by the correction of the wave spectrum. Based on these assumptions, the coefficients $A$ and $B$ for the swell regime are chosen as:

$$A = \left(\frac{H_s^a}{H_s^b}\right)^2 B \text{ and } B = \Delta B \sqrt{\frac{H_s^a}{H_s^b}} \tag{4}$$

With $\Delta B \approx 1$. Because of the swell steepness conservation, this approach seems consistent, because a more energetic spectrum will generally also have a lower peak frequency, and increasing the energy without decreasing the peak frequency produces a swell with an unrealistic steepness.

The second part concerns the assimilation of SWIM parameters from the directional spectra based on Aouf et al. (2019). This part consists mainly of assimilating the two wavenumber components (North-South and West-East components) of dominant wave trains. The procedure consists of the following steps. First, the partitioning is applied to split the model and observation spectra into dominant wave systems called partitions (Gerling, 1992), followed by cross-assignment between model and observation spectra describing the same sea state component, which can be wind sea or swells. The cross assignment follows the method proposed by Hasselmann et al. (1997). An optimal interpolation is then applied between model and observation for the mean wavenumbers of the wave components, to obtain analyzed wave partitions. The final step consists in reconstructing the analyzed wave spectrum by superimposing the analyzed partitions and filling the gaps between partitions by interpolation. The correlation model for optimal spectrum interpolation uses a variable correlation length, which helps to take into account the prevailing sea state. The correlation length varies between 150 km for high latitudes which are dominated by wind-driven sea states, and 450 km for tropical latitudes, which are characterized by a swell-driven sea state (Semedo et al., 2011). The MFWAM model assimilation system, which is operational since February 2021 for assimilation of wave spectra from the Envisat and Sentinel-1 SAR wave mode has been adapted for the assimilation of SWIM wave spectra, taking into account the azimuthal cut-off wavelength of SWIM spectra, which is taken to be equal to 60 m.

The assimilation system is based on the optimal interpolation scheme implemented in the operational wave forecasting system of Météo France. The optimal interpolation consists of computing the appropriate corrections at the observation locations and then spreading them over the model grid points. For this reason, a correlation model depending on the errors of observations and model, and a simple gaussian distribution of the corrections over grid points (spatial scale), are defined (Kalnay, 2002). The weights assigned to the optimal analysis are chosen as follows:

$$W = \mathrm{PH}^T\left[\mathrm{HPH}^T + R\right]^{-1} \tag{5}$$

Where $P$ and $R$ are respectively the correlation function model and the relative error between the errors of observation and model, while $H$ is a matrix that performs the necessary transformation and interpolation of model variables to observation space. By considering the background error homogeneous and isotropic, we express $P$ and $R$ as follows:

$$P = \exp\left(-\left(\frac{d_{ij}}{\lambda_c}\right)\right) \tag{6}$$

$$R = \frac{\sigma_o^2}{\sigma_b^2} \tag{7}$$

where $i$ and $j$ are respectively the coordinates of the grid points of the model, $d$ is the distance from the observation location to the grid point, and $\lambda_c$ is the correlation length.

Consequently, we can write the optimal analyzed mean wave parameters as follows:

$$X^a = X^b + \sum_i^N W_i \left(X_i^o - HX_i^o\right) \tag{8}$$

where $X^a$ and $X^b$ represent the analyzed and background (first-guess) mean wave parameters (energy, wave numbers) at each model grid point, respectively. Upper index $o$ stands for observations, while $N$ is the number of observations affecting a given model grid point. At each grid point, the weights $W_i$ are calculated to minimize the error variance of the optimal interpolation.

In the following, we examine the performance of the assimilation system on the one hand during the analysis period after each assimilation time step (Section 3) and on the other hand during the forecast period (Section 4), that is, after stopping the assimilation. In the first case, assimilation runs over long periods (3 years) are used, which provide an extensive data set that can be compared to independent observations (altimeter or buoys) to analyze the model performance or shortcomings. In the second case, the persistence of the assimilation impact in the forecast time period is used as an indicator of the assimilation efficiency for the operational wave forecasting system. For this evaluation of assimilation impact during the forecast period, we selected one date, 2021-05-31 21:00, where we stopped the assimilation and we analyzed the evolution of the integrated wave parameters from the model for a time period of 10 days. In the 2 cases, the same wind forcing from the analysis of the IFS atmospheric system of ECMWF is used. The impact is evaluated by analyzing the bias and scatter index of the SWH and of the peak period $T_p$, during a 10-day forecast by using collocated wave observations of either buoys or altimeters—see Section 2.4 and 2.5 for the description of these reference data sets.

### 2.4. Altimeter Wave Data Used for Validation

In this study, the SWH provided by six altimeter missions are used for the evaluation of the SWIM data assimilation impact. These are data from CryoSat-2, HY-2B, SARAL, Jason3, Sentinel-3A and Sentinel-3B. SWH are processed with a 1 Hz sampling, corresponding roughly to a 7 km along-track of the satellite. A quality control on the altimeters SWH is applied depending on threshold values of SWH, standard deviation of SWH and backscattered cross section provided in the level 2 products. SWH values are collected in a time window of 3 hr (±1.5 hr from the model output time) and super-observation corresponds to an average on model grid points with a box size of 25 km. The uncertainties associated with measuring sea state and SWH for altimeters (and wave drifting buoys, whose data is defined below) are around 20 cm standard deviation (more information on measurement uncertainties and errors can be found in GCOS, 2016).

### 2.5. Buoy Wave Data Used for Validation

Data from drifting buoys are also used to assess the impact of assimilation based on parameters other than wave heights, such as peak period, not measured by the altimeters. The buoys used here are the SPOTTER drifting buoys deployed by the SOFAR network (Raghukumar et al., 2019). The coverage of this data set is global although heterogeneous in space: buoy density is relatively low in the tropical band or in the Southern Ocean, but very high in the major ocean currents (North Atlantic and Gulf Stream, Agulhas Current, Kuroshio, etc.). This can be seen in Figure 4 which will be discussed in Section 3.3. These buoys measure surface parameters linked to waves, but also to the ocean or atmosphere, such as SST, atmospheric pressure and wind. For waves, we are interested in the peak period parameter, $T_p$, with a sampling frequency of 1–30 s (frequency of 0.03–1 Hz).

In our study, observation and model output data are interpolated using the nearest neighbor method, and in the same way as when processing altimeter data, buoy observations are collected in a time window of 3 hr (±1.5 hr from the model output time). Such processing was carried out here for SWH and $T_p$.

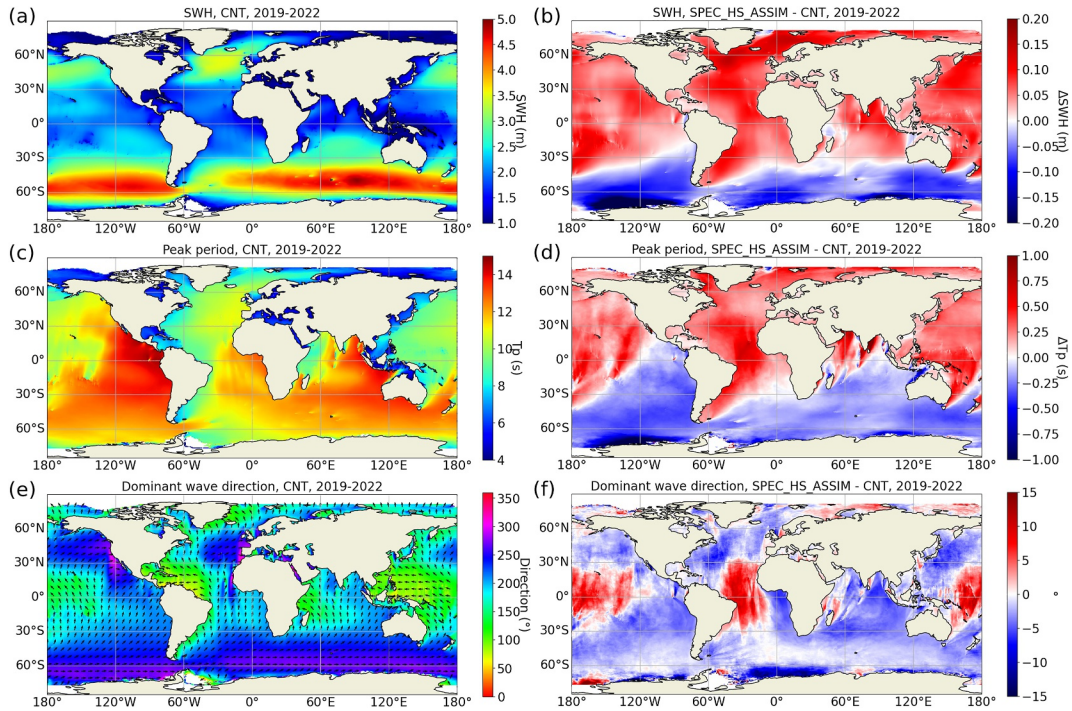


**Figure 1.** Significant wave height, peak period and dominant direction from the CNT run in year 2021 averaged over the 2019–2022 period (a, c, e, respectively) and difference for the same variables between the SPEC_HS_ASSIM and CNT runs in year 2021 averaged over the 2019–2022 period (b, d, f). For the dominant wave direction, the convention is defined as 0° being north and the direction is "from."

From the collocated data set, samples with the peak periods and SWH outliers were first filtered out. It is worth mentioning that peak period is a very sensitive and unsteady parameter in particular due to different frequency discretization applied for the wave spectrum of the model and wave buoy. To get the best reliability and benefits of this data, only waves with SWH between 0.2 and 13 m and peak periods between 4 and 20 s are used in the statistical analysis. We also applied a threshold on the absolute value of peak period bias of smaller than 4 s. All out of range data are rejected as outliers.

## 3. Results

### 3.1. Differences Induced by SWIM Data Assimilation on Wave Parameters

The simulations conducted in this study provide integrated wave parameters that describe the sea state over the global ocean. Figures 1a–1e shows for the CNT model run, the mean values (averaged over year 2021 the 2019–2022 period) of SWH, peak period and dominant wave direction respectively, while Figures 1b–1f shows for the same variables, the mean difference between the SPEC_HS_ASSIM and CNT runs. This characterizes the increment of the model variables due to the joint assimilation of SWH and wavenumbers. First of all, it should be noted that Figures 1a–1f are consistent with results from Semedo et al. (2011), Timmermans et al. (2020), or Hanley et al. (2010).

The mean SWH for the year 2021 the 2019–2022 period illustrated in Figure 1a, indicates high SWH in severe storm ocean areas characterized by strong winds, such as the Southern Ocean, the North Atlantic ocean, and the North Pacific ocean. In addition, ocean regions affected by swell propagation are easily observed in the eastern and northeastern Pacific ocean, the northeastern Atlantic ocean, and the Gulf of Guinea. Figure 1b shows that South of 30°S, SWHs from the SPEC_HS_ASSIM run are smaller than those from the CNT run, by roughly 10 cm on average in the Southern Ocean and up to 20 cm locally, near the Marginal Ice Zone (MIZ). These differences induced by assimilation can probably be explained by a compensating effect of the overestimation of the wind forcing. Indeed, it is known that winds from the IFS ECMWF are overestimated in the Southern Ocean (see Appendix B). Elsewhere, that is, North of 30°S, the average difference is positive indicating that SWH from

10.1029/2025EA004743



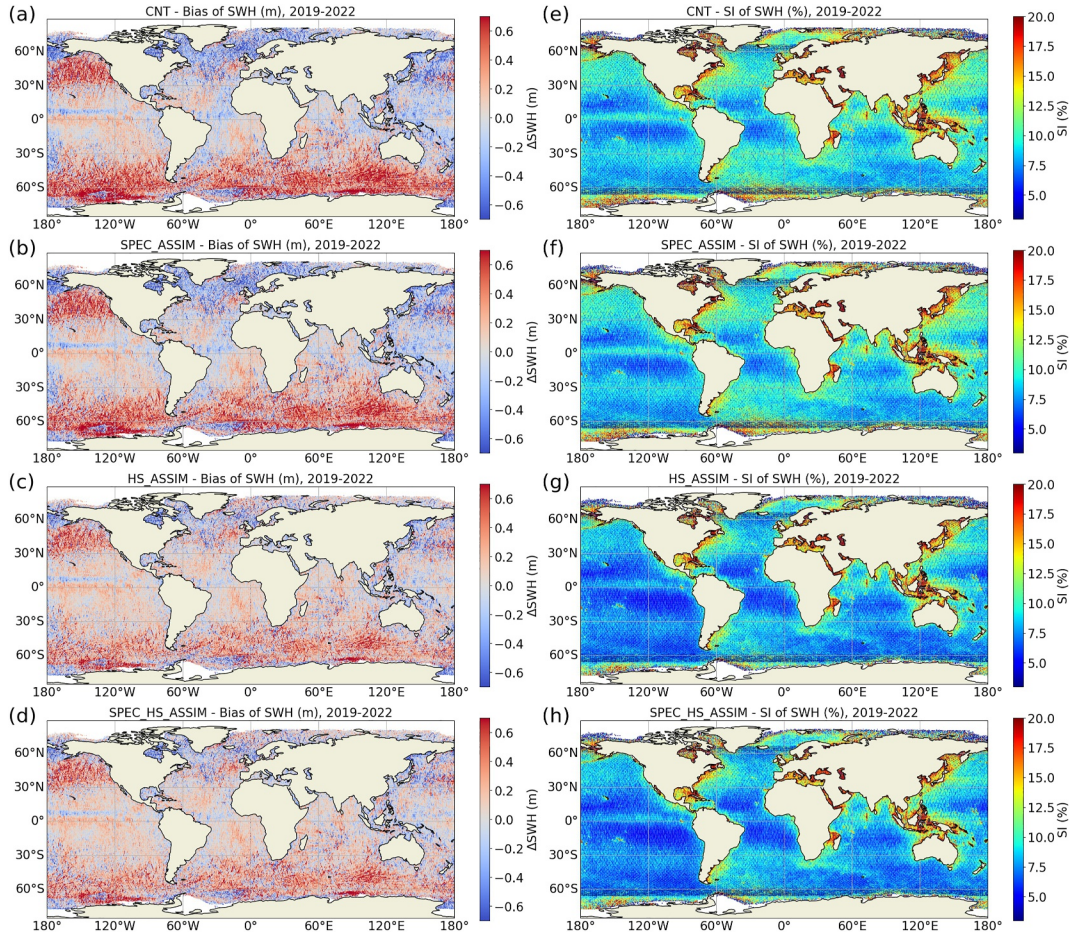


**Figure 2.** Global distribution of bias (a–d) and scatter index (e–h) of SWH in comparison with altimeters SWH in 2021 over the 2019–2022 period. (a)–(d) stand for CNT, SPEC_ASSIM, HS_ASSIM and SPEC_HS_ASSIM respectively. (e)–(h) stand for CNT, SPEC_ASSIM, HS_ASSIM and SPEC_HS_ASSIM respectively.

the SPEC_HS_ASSIM run are larger than those from the CNT run. In this case, there is no clear relation with the wind bias shown in Appendix B.

The averaged peak period for year 2021 the 2019–2022 period from the CNT run is illustrated in Figure 1c. It shows that ocean regions dominated by very long period waves ($T_p$ > 14 s) are mainly located in the tropical eastern Pacific ocean (coast of Mexico) and close to the southern California coasts. It is known that these regions are dominated by swell systems which have propagated from the Southern Ocean region after escaping big storm areas (see e.g., Semedo et al., 2011). In contrast, the smallest peak periods are observed in the enclosed seas of the Northern Hemisphere (up to 5 s on average). Figure 1d reveals a clear separation between regions with the negative and positive increments induced by assimilation. In the Southern Ocean and in a large part of the southern hemisphere basins, the assimilation leads to a decrease of the model peak period. According to the wave climatologies described in Hanley et al. (2010), this corresponds to regions of wind waves generated in the Southern hemisphere and of swell which propagated from these regions to the North-East (see also the wave dominant direction Figure 1e). When comparing with Figure 1b, it can be seen that for the model without assimilation (CNT), both the SWH (i.e., the wave energy), and peak period in the Southern Ocean are larger compared to the model with assimilation (SPEC_HS_ASSIM). Because of the transformation of wind waves in swell, this combined overestimation effect can be observed over most of the regions dominated by the swell generated in the Southern ocean. It appears that assimilating SWIM data has a particular effect on these very long waves, by reducing their peak period, and that this new description from the MFWAM model constrained with SWIM observations a better description thanks to SWIM data of their initial state in the Southern Ocean, where they are generated (at the windward sea stage), enables these properties to be preserved throughout the wave's

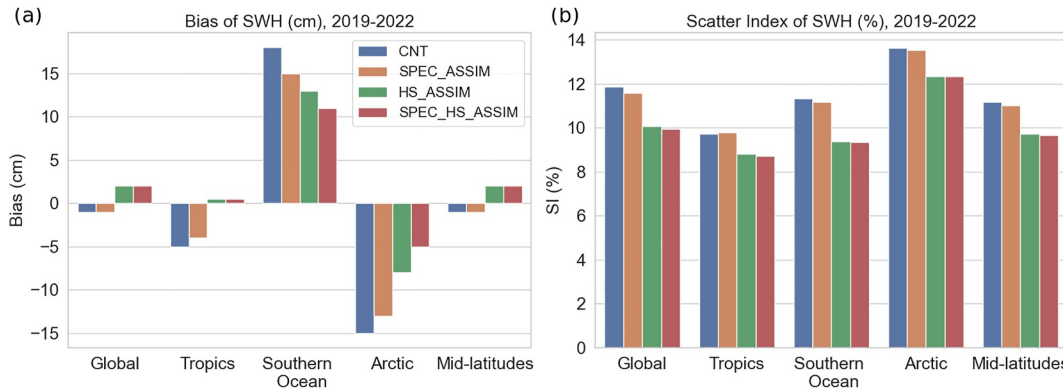


**Figure 3.** (a) Bias and (b) Scatter Index (SI) for SWH in global and typical ocean regions during the period 2019–2022, compared with altimeter observations. Note. The different oceanographic regions are defined by latitude as follows: Tropics: $20°S < \Phi < 20°N$; Southern Ocean: $\Phi < 50°S$; Arctic: $\Phi > 50°N$; Mid-latitudes: $20° < |\Phi| < 50°$.

propagation. Outside this region, the dominant impact of assimilation is an increase of $T_p$, also combined with an increase of SWH, but there is no clear relation with the mean wind bias. The mean absolute difference is roughly about 0.5 s, but maximum values reach 1 s locally.

The dominant wave direction is illustrated in Figure 1e for the CNT run. In the Southern Ocean, the sea state is dominated by westerly waves, with a noticeable directional shift near the Margin Ice Zone (MIZ) of Antarctica. Figure 1e also highlights south-westerly swells approaching the western European coasts, as well as south-westerly swells from the Southern Ocean that impact the Baja California and the west coasts of Central and South America. The ocean regions most affected by directional changes induced by the SPEC_HS_ASSIM run are the tropical zones in the Atlantic and Pacific Oceans. In these areas, the average difference in dominant wave direction, as illustrated in Figure 1f, shifts by approximately 13° clockwise—toward the west—and can reach up to 20° in specific locations. The positive values of the average difference in dominant wave direction are associated with wind waves or young swell regions characterized by an average peak period of 10 s, as observed in Figure 1c. In contrast, the most negative corrections mainly occur along the Antarctica MIZ, and in long swell areas, such as the North East Pacific, and Gulf of Guinea. These waves, originally coming from the west or even the northwest, exhibit a slight directional shift toward the west-southwest due to the assimilation of SWIM data.

### 3.2. Comparison of Model Results Against Significant Wave Heights From Altimeters

The impact of the assimilation is evaluated by analyzing the mean bias, scatter index of the difference between 3-hourly model analysis outputs and altimeter data from HY-2B, SARAL, Jason3, CryoSat-2, Sentinel-3A and Sentinel-3B. The definition of the statistical parameters are recalled in Appendix A.

Figure 2 shows the global distribution of bias and scatter index of SWH for the period of 2021 and for the four runs: CNT in Figures 2a and 2e, SPEC_ASSIM in Figures 2b and 2f, HS_ASSIM in Figures 2c and 2g, and SPEC_HS_ASSIM in Figures 2d and 2h. The model run without assimilation (CNT) indicates a strong overestimation of SWH in the Southern Ocean. As mentioned in Section 3.1, this is most likely because of the overestimation of the 10-m wind forcing from the atmospheric model. This is clearly indicated in Appendix B (Figure B1) and we see that IFS model winds when compared to scatterometer winds show a positive bias, in the Southern Ocean. This positive bias in SWH is also observed in response to the overestimation of the wind speed in the North Pacific Ocean. In contrast, negative bias of SWH with respect to altimeter data up to −50 cm are found with the control run in regions of high currents (Gulf stream, Kuroshio) and close to the sea ice. This is possibly due to not accounting for wave/current and wave/ice interactions in the used version of the MFWAM model. The scatter index corresponding to the control run CNT is the lowest in the Tropics, except at the Equator. The highest values are found in short fetch areas: in enclosed seas, coastal areas and close to the sea ice, where it can reach up to 17%. High values of scatter index are also found in regions of high currents (Gulf Stream, Kuroshio, Atlantic sector of the Antarctic Circumpolar Current). These values are attributed to the same reasons as explained above for the bias.

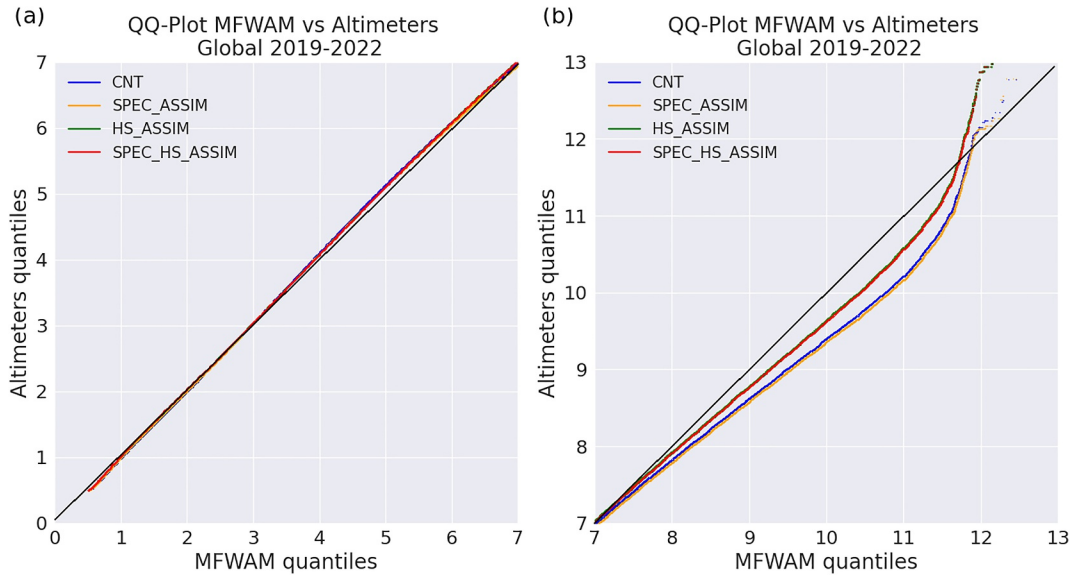


**Figure 4.** QQ-plot for SWH (a) below 7 m and (b) above 7 m for MFWAM quantiles for the four experiments compared to altimeters quantiles over the 2019–2022 period. CNT is represented in blue, SPEC_ASSIM in orange, HS_ASSIM in green and SPEC_HS_ASSIM in red. Perfect fit ($y = x$) is represented as the black line.

When assimilation is activated, the bias on SWH is reduced in the regions where the highest biases were encountered with CNT, and mainly for the HS_ASSIM (Figure 2c) and SPEC_HS_ASSIM (Figure 2d) cases. In contrast, Figure 2 shows that CNT (Figure 2a) and SPEC_ASSIM (Figure 2b) have similar SWH biases, and that HS_ASSIM (Figure 2c) and SPEC_HS_ASSIM (Figure 2d) have the same behavior considering the bias reduction. This reveals that the contribution of SWH assimilation is the most important for the correction of SWH bias and that the assimilation of wavenumbers components is not very efficient to reduce SWH biases. By comparing the case HS_ASSIM with CNT, we see that the reduction of bias is larger in areas of strong currents (the Agulhas, Kuroshio, Gulf Stream and North Atlantic currents, and the Antarctic Circumpolar Current). The basins with the largest bias reduction are the polar oceans, the Arctic and Southern Oceans. Regarding the scatter index, as for bias, it is not reduced in SPEC_ASSIM relative to CNT run. Thus, the assimilation of wavenumbers only is not efficient to reduce the scatter index. However, there is a visible reduction of the scatter index for HS_ASSIM and SPEC_HS_ASSIM relative to SPEC_ASSIM and CNT, so when SWH are assimilated, which is in line with the conclusions on bias above. By comparing the HS_ASSIM and CNT simulations, the highest reduction of scatter index is in the Tropics, in mid-latitudes, and in all the sectors of the Southern Ocean, especially the Atlantic sector.

Figure 3 displays, for year 2021, the statistical parameters at the global scale and for several oceanic regions corresponding to Figure 2. We define the following ocean regions depending on latitudes: Tropics: $-20°$ S $< \Phi <$ 20°N; Southern Ocean: $\Phi < -50°$S; Arctic: $\Phi > 50°$N; Mid-latitudes: $20° < |\Phi| < 50°$. At the global scale, the mean bias on SWH associated with the control run ($-1$ cm) is either similar (for SPEC_ASSIM) or is slightly increased to 2 cm for SPEC_ASSIM and SPEC_HS_ASSIM. But, Figure 3 also shows that the SWH biases differ from one region to the others. When no assimilation is applied (CNT run), the smallest SWH bias is in the tropical ocean regions, while the largest are observed in the Southern Ocean and Arctic ocean. Whereas Mid-latitudes ocean regions show intermediate SWH bias values. When assimilation of SWH is considered (HS_ASSIM and SPEC_HS_ASSIM runs), the highest bias reduction compared to the CNT run is in the Arctic ocean for the SPEC_HS_ASSIM case (bias reduced from $-15$ to $-5$ cm). For the tropics and mid-latitude ocean regions, the impact of the assimilation on the mean bias is small, because CNT run already performs accurately small bias. In the Southern Ocean, although the SWH bias is reduced for all assimilation runs compared to the CNT run, a mean positive bias remains, even for the best cases, with a bias reduction from 18 cm for CNT to 13 and 11 cm for the HS_ASSIM and SPEC_HS_ASSIM cases, respectively. This remaining bias means that none of these assimilation runs can fully compensate for the uncertainties due to wind overestimation of the IFS atmospheric model forcing. It is also interesting to note that in this region of the Southern Ocean, the SPEC_ASSIM run leads to a reduction of the

SWH bias although SWH is not assimilated in this run. Adding the assimilation of SWH from SWIM nadir observations in SPEC_HS_ASSIM decreases even more the bias compared to SPEC_ASSIM.

As concerns the Scatter Index (SI) of SWH, its global value varies between 10.5% and 13.6% depending on the assimilation experiment (13.6% for the CNT run). It is reduced for all assimilation runs compared to the CNT run. The largest reduction of SI of SWH is for HS_ASSIM and SPEC_HS_ASSIM whereas for SPEC_ASSIM, the reduction is only marginal compared to CNT run. It shows again that most of the reduction of the SI of SWH is driven by the assimilation of SWH, and that this latter dominates in the error reduction when it is combined with the assimilation of wavenumbers (SPEC_HS_ASSIM). The impact of the assimilation on SI of SWH also varies depending on the ocean regions of interest. A reduction of the SWH SI compared to CNT run is found with HS_ASSIM in the Southern Ocean (18% relative reduction of SI—from 11.3% to 9.3%), in the mid-latitudes (13.4% relative reduction of SI—from 11.2% to 9.7%), and in the Tropics (10.3% relative reduction-from 9.7% to 8.7%). The reduction of SI with HS_ASSIM is less important in the Arctic (9.2% from 13.6% to 12.35%). Results for SPEC_HS_ASSIM are almost similar as those from HS_ASSIM in all the ocean regions, whereas the reduction of SI for the SPEC_ASSIM run is small, indicating again that assimilation of wavenumbers without assimilating SWH is not skilled on impacting SWH.

Figure 4 shows the QQ-plots (quantile per quantile plots) for each MFWAM run, relative to altimeter observations for the 2019–2022 period 2021 at the global scale The extreme values are the most interesting and challenging in terms of an operational wave forecasting as they cause the most damages and are also the most difficult to predict using numerical models. As shown in Figure 4a, for the low to intermediate values of SWH (up to 7 m), the quantiles are similar for all the MFWAM experiments and consistent with the quantiles observations. The four experiments show a very slight underestimation for SWH 4 and 6 m, although the SPEC_HS_ASSIM and HS_ASSIM experiments remain the experiments whose lines are nearest to the reference line $y = x$. Figure 4b focuses on extreme values (SWH > 7 m). All four experiments show an overestimation against altimeter observations for very high SWH values; that is, above 7.5 m. The largest overestimation is for waves between 10 and 11.5 m. Also we find for the different runs the same behavior as previously described: the quantiles of the CNT (in blue) and SPEC_ASSIM (in orange) experiments have similar distributions compared to the quantiles of the observations. HS_ASSIM (in green) and SPEC_HS_ASSIM (in red) also have a similar distribution of their quantiles and are closer to observation quantiles compared to CNT and SPEC_ASSIM. Thus, HS_ASSIM and SPEC_HS_ASSIM are more efficient at correcting these extreme values than SPEC_ASSIM in relation to the observations. This again shows the important contribution of SWH assimilation in reducing deviations from observations, and more particularly for the extreme SWH values in the tail of the distribution, around 11 m. Indeed, for SWH values above 11 m, the HS_ASSIM and SPEC_HS_ASSIM runs improve the representation of these high SWH, which is not the case for CNT and SPEC_ASSIM. One can note that this pattern does not seem to apply to SWH > 12 m. However, these extreme SWH are very rare and highly improbable events, and therefore occur infrequently. A more representative sample of this SWH range would therefore be needed to assess the model's performance with assimilation of SWIM data in regard to the detection of these extreme waves.

These QQ-Plots are consistent with Figure 3 in terms of scatter index. HS_ASSIM and SPEC_HS_ASSIM have smaller scatter index than SPEC_ASSIM and CNT, which is reflected here in a better consistency at the extremes of the quantiles of HS_ASSIM and SPEC_HS_ASSIM compared to observations than those of SPEC_ASSIM and CNT for every area described in Figure 3. However, the relationship is not so obvious in terms of bias. When comparing with Figure 3, it is interesting to note that at the global scale SPEC_ASSIM and CNT have a very slightly smaller bias compared with HS_ASSIM and SPEC_HS_ASSIM (3 cm), which is not reflected by the QQ-Plots. Indeed, Figure 4b shows that extreme SWH values (above 11 m) are well corrected thanks to the assimilation with HS_ASSIM or SPEC_HS_ASSIM. Thus, compared with Figures 1 and 3, it appears that the SWH bias that remains is attributable to waves between 8 and 11 m, which are the least well corrected by SWH assimilation.

### 3.3. Comparison of Model Results Against Buoy Measurements

Figure 5e shows the global distribution of the mean SWH from the drifting buoys, where we can see that SWH values exceeding 6 m are located in the Southern Ocean, North Atlantic ocean and Pacific ocean. Figures 5a–d shows the SWH bias maps from the different simulations during the year 2021. Without assimilation (CNT run), the MFWAM model underestimates SWH, particularly in the North Pacific and the North Atlantic regions. This

10.1029/2025EA004743

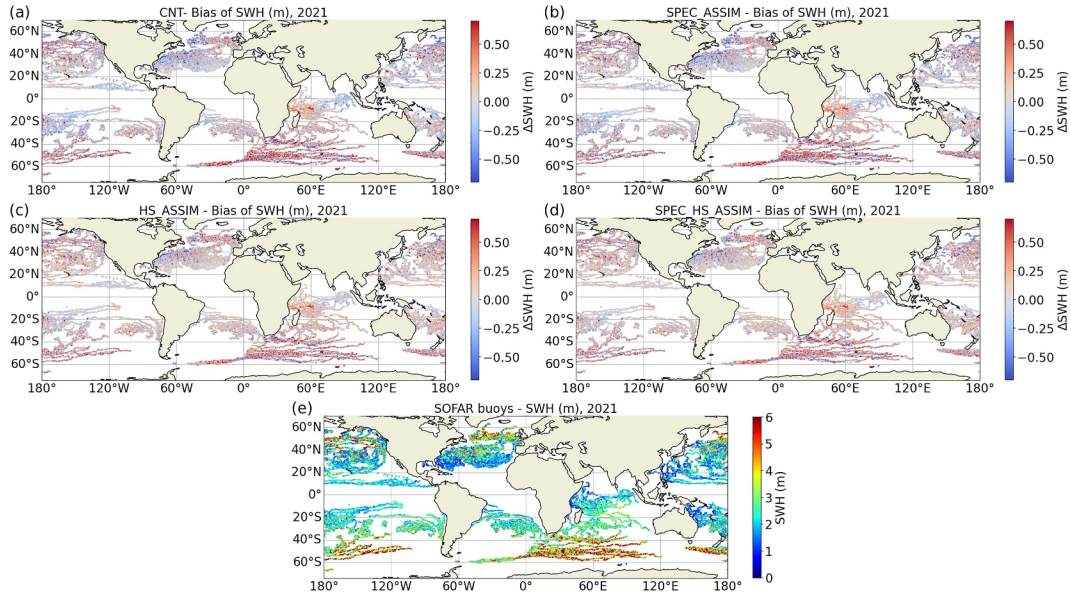


**Figure 5.** Maps of mean SWH bias from the model with respect to SOFAR buoys in 2021. (a)–(d) stand for model CNT, SPEC_ASSIM, HS_ASSIM and SPEC_HS_ASSIM, respectively. (e) Shows the mean SWH from the SOFAR drifting buoys.

negative SWH bias is reduced with the assimilation of SWH from SWIM (both HS_ASSIM and SPEC_HS_ASSIM). In the Southern Ocean, the CNT run leads to a positive bias, consistently observed for the comparison with altimeters data. Moreover, with HS_ASSIM and SPEC_HS_ASSIM this SWH bias is reduced compared to CNT run. SPEC_ASSIM also indicates a bias reduction compared to CNT run but of less amplitude. This figure is consistent with Figure 2 in Section 3.2, comparing SWH in MFWAM with SWH from altimeters.

Statistical analysis on SWH and peak periods are displayed in Figure 6, at the global scale for the same regions as those defined in Figure 3. For the CNT run, the biases are similar to those obtained when using the altimeter data as reference. The largest SWH bias of the CNT run is still found in the Southern Ocean (about 13 cm on average). In the other ocean regions it is rather small (in the Arctic about −5 cm compared to the −15 cm found when comparing to the altimeter data). With SWH assimilation (HS_ASSIM), the SWH bias reduction compared to the CNT is the most effective in the Southern Ocean region, with a reduction from 13 to 10 cm, and in the Arctic, with a reduction from −5 to 1 cm. Concerning SPEC_ASSIM, it is interesting to note that in the Southern Ocean, it has a very close impact from HS_ASSIM for the bias reduction (from 13 to 9 cm). This is consistent with the comparison with altimeters indicated in Figure 3. The impact of the joint assimilation of SWH and wavenumbers components (SPEC_HS_ASSIM) is generally similar to that of HS_ASSIM, except in the Southern ocean where the SWH bias reduction is more pronounced compared to HS_ASSIM and SPEC_ASSIM. This confirms the same results of the comparison with altimeters.

The SI of SWH is reduced in all regions with SPEC_ASSIM, HS_ASSIM and SPEC_HS_ASSIM compared with CNT. The impact of SPEC_ASSIM is smaller but positive in terms of SI reduction, although it remains close to SI of CNT. By separating the different contributions of SWH (HS_ASSIM) and wavenumbers (SPEC_ASSIM) assimilation, the assimilation of SWH is the most effective in reducing SWH scatter index, for all regions. However, it is by combining the two types of observations (in SPEC_HS_ASSIM) that we achieve the best scatter index reduction compared with CNT. This is visible in all areas. It should be noted, however, that in the Southern Ocean, the scatter index of HS_ASSIM is very close to that of SPEC_HS_ASSIM, but still slightly smaller. This is consistent with the comparison with altimeters, where the two scores were also found to be similar in the Southern Ocean.

Figure 6 also shows the statistical parameters for the peak period ($T_p$). For the CNT run, the peak period exhibits a mean bias with respect to buoy observations of 0.25 s at the global scale, varying from −0.05 s in the Arctic ocean to 0.64 s in the Southern Ocean, and intermediate values obtained in the other ocean regions (0.36 and 0.23 s in the

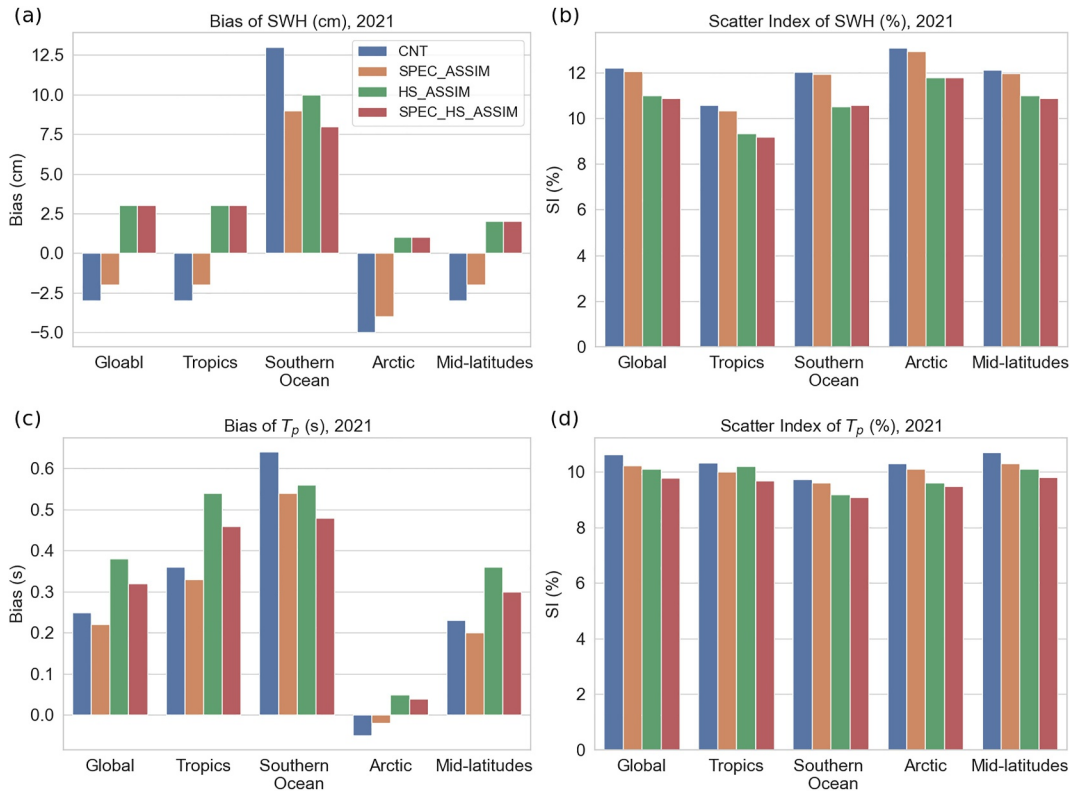


**Figure 6.** Statistical parameters for SWH and $T_p$ in global and typical ocean regions in 2021, compared with SOFAR buoys observations. (a) Stands for SWH bias, (b) is the SI of SWH, (c) is the $T_p$ bias, and (d) is the SI of $T_p$. Note. The different oceanographic regions are defined by latitude as follows: Tropics: 20°S < Φ < 20°N; Southern Ocean: Φ < 50°S; Arctic: Φ > 50°N; Mid-latitudes: 20° < |Φ| < 50°.

Tropics and mid-latitudes regions, respectively). From Figure 6, it is clear that HS_ASSIM run degrades the model peak period accuracy, in terms of $T_p$ bias, compared to drifting buoy observations, except in the Southern Ocean where an improvement is observed (bias decreases from 0.64 s in CNT to 0.56 s for HS_ASSIM). SPEC_ASSIM run always improves the bias compared to CNT. The degradation of the peak period associated with SWH assimilation is linked to Lionello's spectrum correction method (1992), which is based on an approximation consistent with the physics of the wave model, in this case MFWAM. This is performed via the parameter B in Equations 3 and 4, which adjusts the intensity of the correction applied to the spectrum and determines the redistribution of energy across all frequencies. This redistribution modifies the shape of the spectrum. The average frequency is related to the total integrated energy, and the peak frequency to the maximum energy of the spectrum. Thus, a correction of Hs can improve the average frequency while inducing a shift in the peak frequency (or period). This effect is particularly pronounced in wind sea situations, where the sea state is generally more dependent on the non-linear wave-wave interactions and white-capping dissipation processes. Therefore the computation of the peak period is very sensitive to corrections on the average frequency induced by the assimilation of SWH. At the global scale, the bias reduction is about 12% for SPEC_ASSIM relative to CNT, while the degradation of bias with respect to CNT reaches 52% for HS_ASSIM, and 28% for SPEC_HS_ASSIM. This shows that the assimilation of wavenumbers is efficient to correct the large bias of $T_p$ but that this efficiency is affected when the assimilation of SWH is included. The assimilation of SWH generally tends to increase the bias of the peak period. However, the assimilation of both wavenumbers and wave heights (SPEC_HS_ASSIM) still gives reduced biases compared to the assimilation of SWH alone (HS_ASSIM) in every ocean region.

The scatter index for the CNT run is between 9.75% and 10.7% depending on the region. As with the peak period bias, the SI of HS_ASSIM, SPEC_ASSIM and SPEC_HS_ASSIM are reduced compared with CNT. If we consider separately the contributions of the assimilation of the SWH and the wavenumbers, it is the SWH assimilation (HS_ASSIM) that is the most effective everywhere except in the Tropics. In the Tropics,

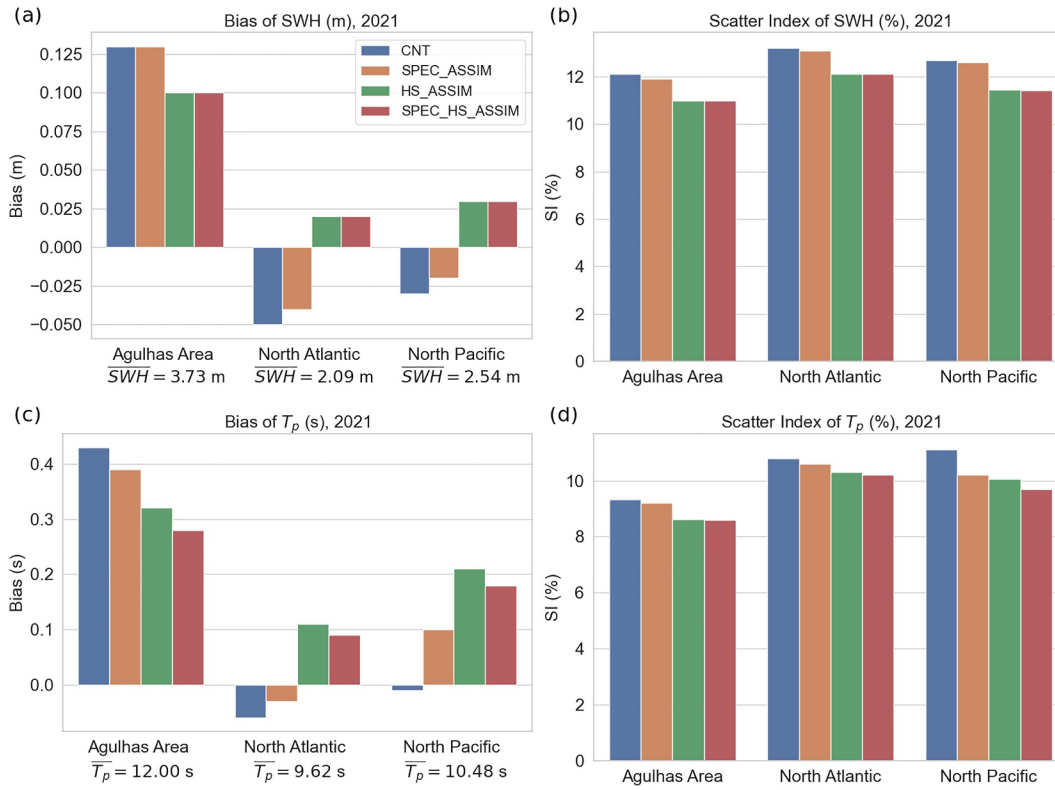


**Figure 7.** Statistical parameters for SWH and $T_p$ in areas of high density of collocated points 2021, compared with SOFAR buoys observations. (a) Stands for SWH bias, (b) is the SI of SWH, (c) is the $T_p$ bias, and (d) is the SI of $T_p$. Mean values of SWH and $T_p$ from SPOTTER buoys are also shown. Note. The different regions are defined by latitude-longitude boxes as follows: Agulhas region (35–50°S, 10–50°E), North Atlantic (30–60°N, 0–60°W) and North Pacific (30–60°N, 130°W–160°E).

wavenumber components assimilation (SPEC_ASSIM) is the most effective in reducing the peak period scatter index. Finally, at global level and for all regions, it is the combination of the two observations (SPEC_H-S_ASSIM) that is most effective in reducing the peak period SI.

In Figure 7, we chose to focus on ocean areas (compared to those in Figures 3 and 6) delimited by the highest density of collocated points. The new regions are defined by latitude-longitude boxes as follows: Agulhas Current (35–50°S, 10–50°E), North Atlantic (30–60°N, 0–60°W) and North Pacific (30–60°N, 130°W–160°E). Figure 7 shows the SWH and $T_p$ bias and scatter index in these areas. These regions are also considered because they are dominated by different sea states and wave regimes, for instance the Northern Atlantic is less dominated by swell compared to other basins.

The SWH bias for CNT run is the largest in the Agulhas region, with 13 cm in average, and the smallest is found in the North Pacific region with—3 cm in average, with an intermediate value of—5 cm in average in the North Atlantic. In the Agulhas region, SPEC_ASSIM run did not reduce the SWH bias, while HS_ASSIM and SPEC_HS_ASSIM runs decreased it by 3 cm. In the North Atlantic, HS_ASSIM and SPEC_HS_ASSIM are the two experiments with the smallest SWH bias, and the assimilation of SWH plays an important role in reducing the bias observed in the CNT run, while assimilation of the wavenumber components has only a very small positive impact on bias reduction. In the North Pacific, all assimilation runs degrade the SWH bias except SPEC_ASSIM, but it slightly reduces the bias by 1 cm on average. Nevertheless, SWH bias is already small for CNT run, it remains very small for SPEC_ASSIM run. For HS_ASSIM and SPEC_HS_ASSIM runs, the SWH bias switches to a positive same value, which is induced by the assimilation of SWH. This also indicates that in this region, assimilating wave numbers components has not been degraded by the assimilation of SWH.

The SI of SWH is the largest for CNT run for all regions, with maximum values for the North Atlantic ocean area of about 13.2%. It is estimated to 12.7% for the North Pacific and 12.1% in the Agulhas region. For all the ocean

regions studied, HS_ASSIM and SPEC_HS_ASSIM have very similar scores and provide the best reduction of SI of SWH compared to CNT. It shows that the most efficient way to reduce the scatter index for SWH is to jointly assimilate the SWH and the wavenumbers components, although the positive effect and the reduction of the SI is dominated by the assimilation of SWH. In the three ocean areas, SPEC_ASSIM run only has a very limited positive effect in the reduction of SI of SWH compared to CNT run.

Regarding to statistical parameters for the peak period displayed in Figure 7, the CNT run leads to large bias in the Agulhas region (0.43 s, representing about 3.6% of the mean value), and is much smaller for the other two ocean regions: −0.06 s in the North Atlantic, and—0.01 s in the North Pacific. In the North Atlantic, the assimilation of wavenumbers components is efficient in reducing the $T_p$ bias. Indeed, SPEC_ASSIM achieves the largest bias reduction. In opposite, the assimilation of SWH degrades the bias, which is about 0.11 s for HS_ASSIM. When SWH and wavenumbers components are jointly assimilated as in SPEC_HS_ASSIM, the bias is smaller than with HS_ASSIM, but it remains relatively high compared to CNT run (0.09 s relative to—0.06 s), indicating that the negative impact of SWH assimilation dominates over the positive effect of the wavenumber components assimilation. In the North Pacific, all the assimilation runs tend to increase the bias compared to the CNT run. The largest increase is for HS_ASSIM (0.21 s instead of −0.01 s in the CNT run), while the smallest is for SPEC_ASSIM (0.10 s). The $T_p$ bias with SPEC_HS_ASSIM run (0.18 s) is smaller than that with SPEC_HS but remains larger than CNT and SPEC_ASSIM runs. The sea state in this area is dominated by mature wind sea or transitioning to swell (average $T_p$ about 10.48 s). We assume that at this stage of the wave's growth, during its transition from windsea to swell, uncertainties in the estimate of the peak period are high due to the different methods of frequency discretization for the drifting buoys and the model wave spectra. Moreover, the source term in MFWAM uses the DIA approximation to resolve nonlinear interactions between waves during growth and transition phases. The parameterization of this source term could also explain some of the uncertainties in estimating the peak period in this region, where nonlinear interactions frequently occur. Finally, the Agulhas region shows interesting results for the different assimilation configurations compared to the other two ocean areas. This is the region with the largest $T_p$ bias for CNT run with 0.43 s (as for the largest SWH bias for CNT run). It is also the only ocean region where HS_ASSIM run does not degrade the $T_p$ bias, but on the contrary improves it compared to CNT run and slightly better compared to SPEC_ASSIM. The Agulhas region is known to be particularly intense in terms of wave-current interactions, where surface currents have a strong impact on wave propagation. However, the model runs did not account for wave/current interactions, which could explain the high $T_p$ and SWH biases of the four simulations and especially the CNT run. The assimilation of SWIM data (SWH and wavenumbers components) seems to correct partly for the error associated with the lack of the wave-current interactions.

The SI of $T_p$ for CNT run is the largest in the North Pacific roughly about 11.1%, and the smallest in the Agulhas region with 9.33%, intermediate value of about 10.8% in the North Atlantic region. For the three ocean areas, CNT run less performs in terms of $T_p$ SI compared to the assimilation runs. SPEC_ASSIM reduces slightly the SI of $T_p$ compared to CNT run, followed by HS_ASSIM. For all ocean regions, SPEC_HS_ASSIM run leads to the best performance for $T_p$ SI and the smallest SI. It is noteworthy to mention that HS_ASSIM run has the second best performance of SI of $T_p$.

In complement we discuss with Figure 8 the impact of assimilation on SWH as a function of SWH bias and $T_p$. Figure 5 shows the variation of SWH bias between model runs and buoys, against the buoy SWH value (horizontal axis), with buoy peak periods identified by the color bars.

In the Agulhas region (Figures 8a–8c), the CNT run less performs in terms of orthogonal regression between the SWH bias and different range of SWH. SPEC_ASSIM runs shows similar regression coefficients, consolidating the conclusions from Figure 7 about the very small impact of the assimilation of wavenumber components on reducing SWH bias in this area. Among the model runs, HS_ASSIM shows the lowest slope and intercept, indicating the best performance. Adding wavenumbers components in SPEC_HS_ASSIM run only slightly affects and even degrades these results. These figures enable us to analyze SWH biases as a function of SWH ranges and the impact of the different assimilation on the biases variations, rather than only analyze the mean bias in Figure 7. According to the regression fit, CNT run has a bias of 0.4 m on 2 m waves, and - 0.5 m on 10 m waves. The runs with SWH assimilation, HS_ASSIM and SPEC_HS_ASSIM runs, correct the best these biases for both SWH scales: the bias for these runs is 0.2 m and—0.4 m for 2 and 10 m waves, respectively. The SPEC_ASSIM run does not reduce the bias compared with CNT run, for all SWH scales. It should be noted, however, that there

10.1029/2025EA004743



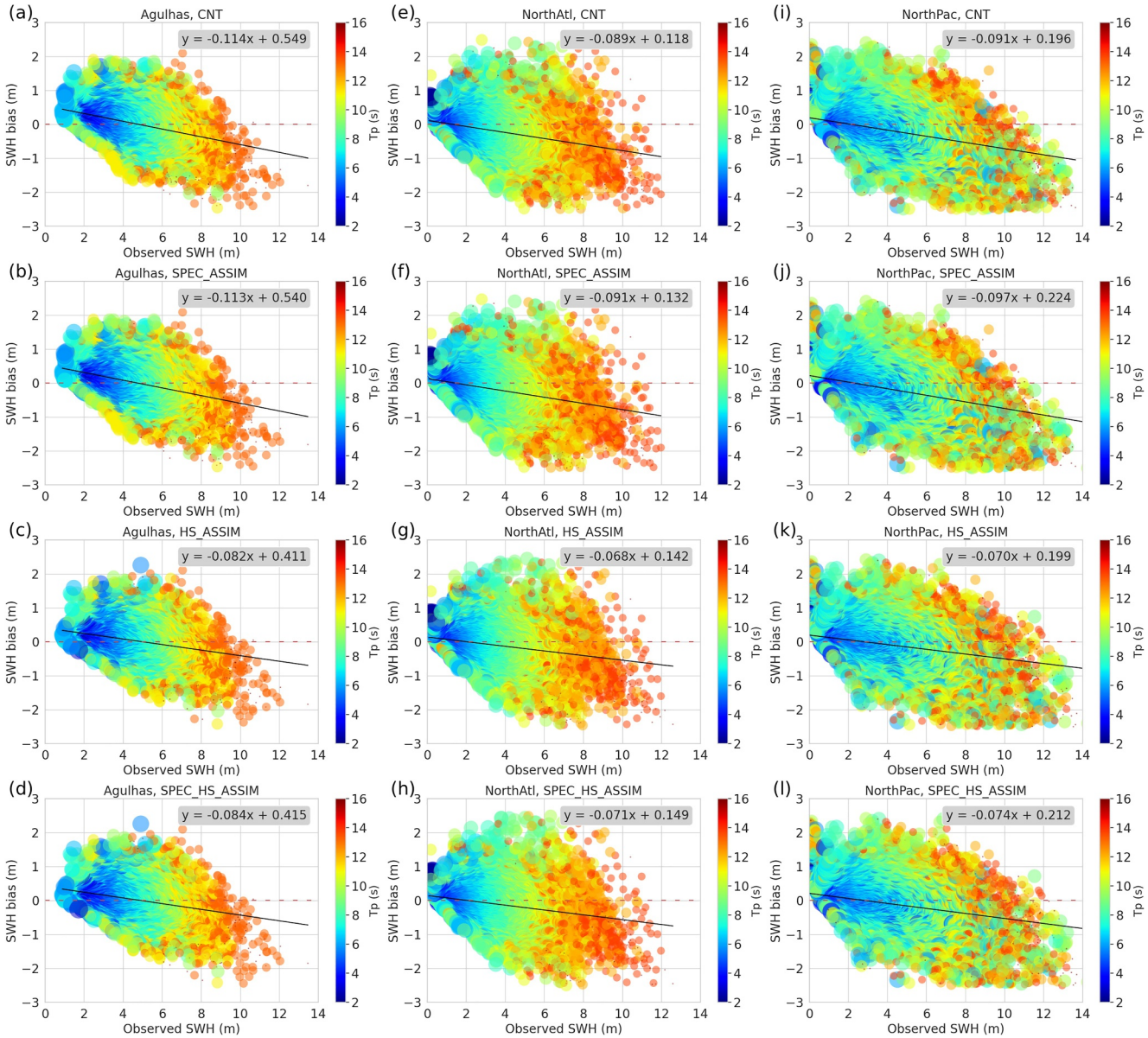


**Figure 8.** Variation of SWH bias with SWH and peak period in comparison with SOFAR wave buoys during the year of 2021. (a)–(d) stand for CNT, SPEC_ASSIM, HS_ASSIM and SPEC_HS_ASSIM corresponding to the Agulhas Current (35–50°S, 10–50°E), respectively. Whereas figures (e), (f), (g) and (h) indicate CNT, SPEC_ASSIM, HS_ASSIM and SPEC_HS_ASSIM corresponding to the North Atlantic (30–60°S, 0–60°W), respectively, and finally (i)–(l) indicate CNT, SPEC_ASSIM, HS_ASSIM and SPEC_HS_ASSIM corresponding to the North Pacific (30–60°N, 130°W–160°E). Orthogonal regression fit is indicated by black line and the red dashed line stands for the perfect fit ($y = 0$). To make the figure easier to read, short periods are represented by large blue circles, and long periods by small red circles.

remains a positive bias of 0.2 m on average for low SWH values, and a negative bias of 0.5 m on average for high SWH values, even with SPEC_HS_ASSIM and HS_ASSIM runs. Both HS_ASSIM and SPEC_HS_ASSIM efficiently correct SWH for different scales of $T_p$. Here, assimilation causes a shift in the change in sign of the SWH bias. Indeed, for the CNT and SPEC_ASSIM simulations, the SWH bias changes from positive to negative for SWH of 4.7 m and $T_p$ of approximately 8–9 s, while for HS_ASSIM and SPEC_HS_ASSIM, the bias changes sign for SWH of 5.5 m and $T_p$ of 9–10 s. These peak period values are typical of waves in a growth phase or transitioning from wind sea to swell regimes. This shift in the change of sign of the bias suggests that a redistribution of energy between windsea and swell occurs during the assimilation process, contributing to the correction of the bias. Furthermore, the fact that assimilation simultaneously reduces the bias in windsea and swell

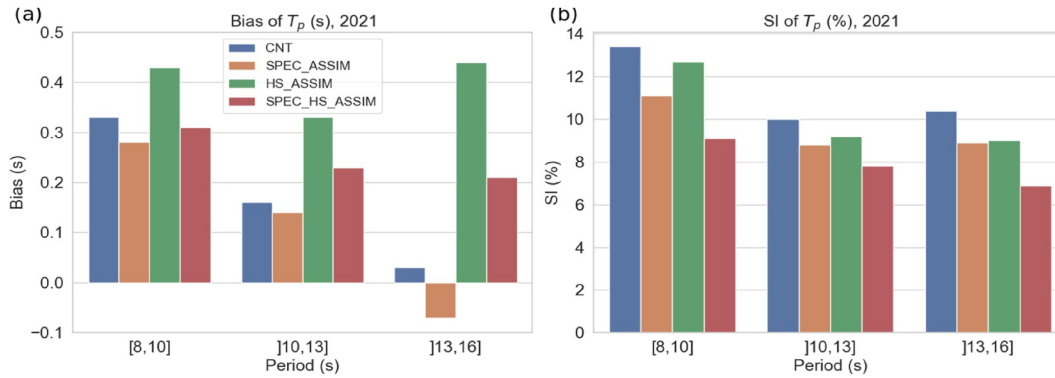


**Figure 9.** Bias (a) and Scatter index (b) of the peak periods from the model compared to the buoy observations at the global scale. Green, blue, orange, blue, green, and red bars stand for CNT, SPEC_ASSIM, HS_ASSIM, SPEC_HS_ASSIM, respectively. The results are shown for three categories of peak period: $8 \leqslant T_p \leqslant 10$ (21.10%), $10 < T_p \leqslant 13$ (36.80%), $13 < T_p \leqslant 16$ (12.70%).

regimes implies that the correction cannot be a single adjustment of the total energy. This behavior suggests that assimilation allows for a redistribution of energy between windsea and swell components. Because of the principle of conservation of swell steepness assumed in the assimilation scheme, following the method of Lionello et al. (1992), changes in SWH and $T_p$ are correlated; if the increment induced by the assimilation for SWH is positive, the same applies for $T_p$, and vice versa. Thus, in this swell-dominated ocean area, assimilation efficiently redistributes energy between windsea and swell, particularly through SWH assimilation. Additionally, because strong currents can influence wave properties, the assimilation of SWH helps to mitigate the bias caused by the lack of wave-current interactions in the model.

In the North Atlantic basin, the wave climate is a lot less dominated by swell from other ocean basins, as indicated on Figure 7 ($T_p$ around 9.62 s). In this basin, the simulation with the best scores in terms of linear regression slope is HS_ASSIM. The intercept coefficient is best for CNT run, but there are high uncertainties for these low SWH values. For these SWH values (<2 m), the bias is equivalent for all 4 runs and averages 5 cm, which is small. This indicates that HS_ASSIM run corrects all SWHs, especially the high SWHs (10–12 m), which correspond to the highest peak periods (14 s). According to the regression fit, the bias for SWH of 10 m reaches—0.7 m for CNT run and—0.7 m for SPEC_ASSIM run and is reduced to—0.5 m for SPEC_HS_ASSIM run and—0.5 m for HS_ASSIM run. This is consistent with Figure 7 and reinforces the conclusion about the efficiency of SWH assimilation in correcting high SWH, as seen in Figure 4. However, we still note this positive systematic bias for low SWH and negative for high SWH.

In the North Pacific region, we can see that sea states are different from the other two basins, with higher SWH, and a sea state dominated by a mature wind sea, with peak periods around 10.48 s, according to Figure 7. The performance of the four runs is close to that obtained in the North Atlantic basin, although more noticeable. For the four runs, biases at SWH < 2 m are small, averaging 5 cm. At high SWH, SWH assimilation still plays the main role in reducing SWH bias, while the assimilation of wavenumbers components seems to be less effective. Indeed, the bias for SWH of 10 m reaches—0.8 m for CNT run and—0.7 m for SPEC_ASSIM run and is reduced to—0.4 m for SPEC_HS_ASSIM run and—0.3 m for HS_ASSIM run. This was also observed in the North Atlantic basin, also dominated by mature wind seas in transition to young swells. So, what was discussed in the Agulhas does not apply here, and Lionello's scheme does not seem to redistribute wave energy correctly during the transition from wind sea to swell and the assimilation of wavenumbers cannot compensate for the bias induced by the assimilation of SWH.

It is also interesting to analyze the impact of assimilation as a function of ranges of $T_p$. To this end, we analyze at the global scale the bias and SI of the peak period in three classes of $T_p$, representing respectively, the presence of intermediate wind waves (peak period 8–10 s), young swell (10–13 s) and long swell (13–16 s). We can see that the SI of $T_p$ compared with drifting buoys is reduced for all classes of $T_p$ and all assimilation experiments compared to CNT run, as illustrated in Figure 9b. The largest reduction of SI of $T_p$ is obtained for SPEC_H-S_ASSIM for all ranges of $T_p$ with the maximum reduction of 34% for $T_p$ larger than 13 s. SPEC_ASSIM and HS_ASSIM give almost the same SI, except for the smallest period bin (8–10 s) where SPEC_ASSIM performs

better than HS_ASSIM. The largest reduction of SI of $T_p$ for SPEC_ASSIM is 13% on average for $T_p$ larger than 13 s, much less than in the case of SPEC_HS_ASSIM. Assimilating the SWHs alone (HS_ASSIM) does not result in a clear reduction for SI of $T_p$ for waves with $T_p$ smaller than 10 and 13 s (only 5% and 8% reduction for HS_ASSIM compared with CNT run).

Regarding the $T_p$ bias (Figure 9a), the impact of the assimilation is more complex. We can see that assimilating SWHs alone (HS_ASSIM) adds a very strong bias for all $T_p$ ranges, with a bias increase of more than 0.4 s for $T_p$ greater than 13 s. This suggests that rescaling the wave spectrum after the assimilation of SWH (Lionello et al., 1992) needs to be adjusted depending on whether the wave regime is wind sea or swell. SPEC_ASSIM run did not show this degradation for the $T_p$ bias; on the contrary, it has been observed a slight reduction in $T_p$ bias (about −12.5%), particularly for waves dominated by young swells, with peak periods between 10 and 13 s. This reinforces the hypothesis that this degradation is due to the limitations of the assimilation procedure when assimilating SWH alone. In the case of SPEC_HS_ASSIM, the assimilation of wavenumbers components is not sufficient to balance the degradation induced by the assimilation of SWH so that the overall effect is to increase the $T_p$ bias for peak periods larger than 10 s (and only marginally decreasing the $T_p$ bias for periods between 8 and 10 s).

The results concerning the bias and SI of $T_p$ across different $T_p$ ranges provide additional insights beyond those presented in Figure 6 and discussed earlier. Indeed, Figure 6 indicates that HS_ASSIM run exhibits the largest bias in $T_p$ (0.60 s) relative to drifting buoy observations. We can now conclude that this bias persists across all $T_p$ ranges above 8 s, with the most substantial increase in bias for waves with peak periods exceeding 13 s, likely due to an incorrect assumption in the SWH assimilation scheme regarding swell steepness conservation. Both Figures 6 and 9a show that the assimilation of SPEC_ASSIM yields the best results. Figure 9a further demonstrates that the $T_p$ bias reduction occurs across all $T_p$ ranges from 8 to 16 s. As previously noted, SPEC_HS_ASSIM run is unable to fully compensate for the negative impact on bias caused by SWH assimilation, especially for $T_p$ above 10 s, as shown in Figure 9a. Nevertheless, it remains effective—similar to SPEC_ASSIM run—in reducing the scatter index across all $T_p$ classes.

## 4. Impact of the Assimilation in the Forecast Period

In this section we performed a statistical analysis on SWH and $T_p$ during the forecast period. Figure 10 shows the time series of the bias and scatter index of the peak period and SWH for all runs after the date when we stopped the assimilation.

Figure 10a shows that the bias of SWH is relatively small for all runs, with an average bias of SWH smaller than 4 cm. The evolution of this bias during the first day of forecast indicates small differences between the runs, and after the third day of forecast the SWH bias is almost the same for all runs. This figure shows a very small SWH bias for the four experiments, less than 4 cm on average. It is then not significant to interpret the impact of the assimilation for such a range of SWH bias. Regarding the evolution of the scatter index of SWH, Figure 10b indicates the efficiency of the assimilation in runs HS_ASSIM and SPEC_HS_ASSIM, both demonstrating the best performance during the first 2 days of forecast. After one day of forecast, the SI of SWH is 10.2% for the ASSIM_HS run and 9.7% for the ASSIM_SPEC_HS run, both significantly smaller than that of the CNT run (roughly ∼11.5%). Interestingly, the SPEC_ASSIM run slightly reduces the SI of SWH compared to CNT run during the first 2 days of the forecast period.

Figure 10c shows the evolution of the bias for the peak period from all runs during the forecast period. We can see clearly that the HS_ASSIM and SPEC_HS_ASSIM runs exhibit a stronger positive bias (respectively 0.26 and 0.3 s after 1-day) than the other runs during the first 4 days of the forecast. Subsequently, this bias of $T_p$ decreases and reaches the same bias of $T_p$ for the CNT and SPEC_ASSIM runs, which is roughly 0.1 s. Interestingly, the SPEC_ASSIM run indicates the smallest bias of $T_p$ between days 5 and 7 of the forecast period. This highlights the benefit of assimilating directional properties of wave partitions as observed by SWIM instrument.

Finally, we look at the time evolution of the scatter index of the peak period after assimilation is stopped, which is shown in Figure 10d. The CNT and SPEC_ASSIM experiments have the largest SI of $T_p$ up to T+2 12 hr, whereas the HS_ASSIM and particularly SPEC_HS_ASSIM runs are the most efficient at reducing the scatter index during this period. We also note that the assimilation runs (SPEC_ASSIM, HS_ASSIM and SPEC_HS_ASSIM) achieve an SI of $T_p$ smaller than 10% between T+1 and T+2 12 hr, which is satisfactory, compared to the CNT control run. After 3.5-day of forecast, all runs indicate a scatter index of $T_p$ of roughly 11.4%.

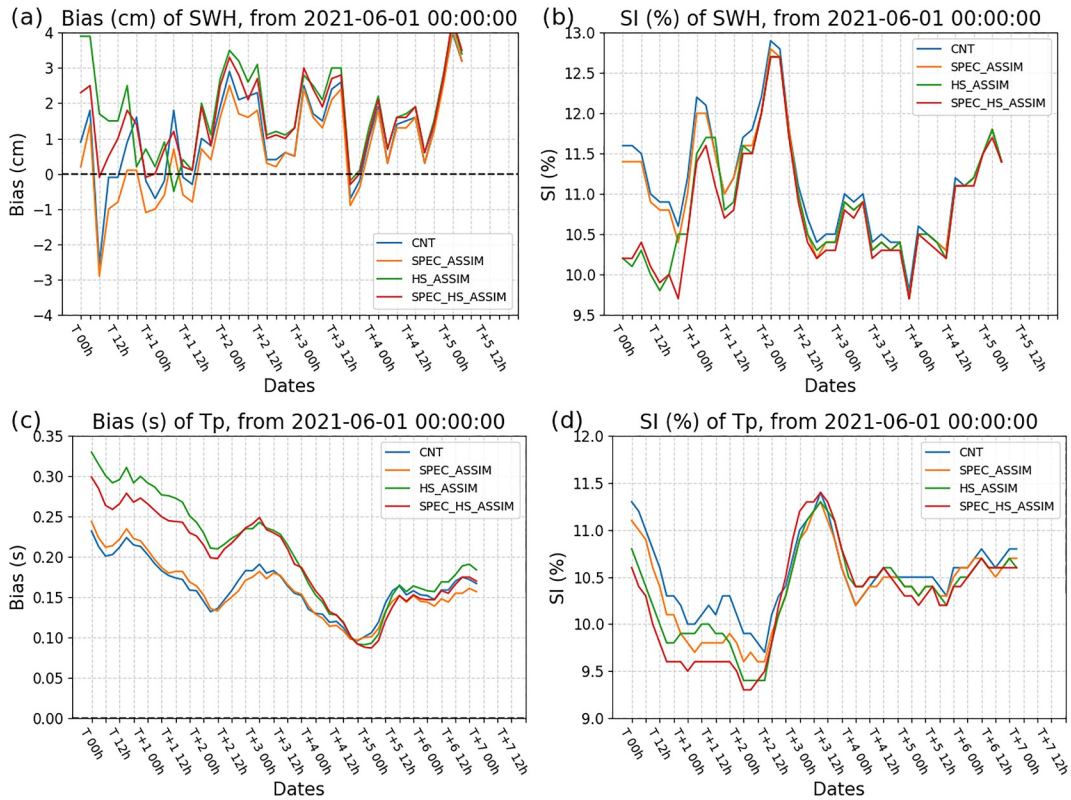


**Figure 10.** Variation of statistical scores of $T_p$ and SWH from the model MFWAM in comparison with drifting SOFAR buoys, during the forecast period. The top line (a, b) stands for the SWH parameter, and the bottom one (c, d) for the peak period. The right column (b, d) stands for the bias and the left one (a, c) stands for the scatter index relative to the observations. Colors blue, orange, green and red stand for CNT, SPEC_ASSIM, HS_ASSIM and SPEC_HS_ASSIM. The forecast period starts on 1 June 2021, 00:00.

More specifically we analyzed the impact of the assimilation during the forecast period for peak periods ranging between 12 and 18 s in the buoy data. This concerns the most energetic swell, which can enhance the risk of dangerous seas in coastal regions and ship routing Statistical analysis in Figure C1 (Appendix C) indicates negligeable $T_p$ bias for SPEC_HS_ASSIM and HS_ASSIM runs, while it is estimated at −0.10 and −0.14 s for SPEC_ASSIM and CNT runs, respectively. We also remarked that the best reduction of peak period SI is obtained for SPEC_HS_ASSIM, with an estimated SI of 11.6% for the full forecast period. This highlights the efficiency of the joint assimilation of SWH and wavenumbers components during the forecast period, with an improvement on average by roughly 13% compared to CNT run. It shows again that for long swells ranging between 200 and 500 m, the benefit of the assimilation of SWIM directional wave spectra is an interesting perspective for operational wave prediction and particularly during storm events.

## 5. Summary and Conclusions

In this study, we evaluated the impact of the assimilation of SWIM wave observations into the MFWAM wave model. The innovative SWIM wave scatterometer provides directional wave spectra that describe windsea and swell, with wavelengths ranging from 60 to 500 m. Four long-term model runs have been conducted to assess the benefits of using SWIM wave data. The assimilation runs showed improvements in estimating integrated wave parameters, such as SWH and $T_p$. This has been evidenced by a reduction in both bias and scatter index of SWH when compared to independent observations for several ocean basins. The results also show some limitations of the assimilation scheme used in the MFWAM model, because of assumptions used in the Lionello et al. (1992) scheme. These limitations are visible when assimilating only SWH or jointly SWH with the wavenumbers components of partitions, with an increased bias on the peak period compared to without assimilation experiment. We also highlight that such an increased bias for $T_p$ can be induced by the different discretization of frequency

scale for the buoys and the model runs. Only the Agulhas current region, dominated by long swells propagating from the Southern Ocean, does not show this increase of the peak period bias, which suggests that the assimilation scheme of SWH is more effective in swell-dominant ocean regions.

The control run without assimilation shows that wave parameters (SWH, peak period, dominant direction) are broadly consistent with the literature (Semedo et al. (2011), Timmermans et al. (2020), or Hanley et al. (2010)). Comparison of the control run with the run with combined assimilation reveals that assimilation reduces SWH south of 30°S, particularly in the Southern Ocean, compensating for the overestimation of IFS winds, while increasing SWH above this latitude. The peak period is reduced by the assimilation in the southern hemisphere and in ocean areas affected by the swells propagation originating in the Southern Ocean. Outside this region, the assimilation tends to increase both SWH and peak period $T_p$ simultaneously, without any direct link to wind biases. For the dominant wave direction, the strongest corrections appear in ocean regions near the MIZ of the Antarctic and in the Tropics, with average directional shifts of around 13° and up to 20° locally. As the tropics are known for a high probability of crossing seas, improved predictability of wave direction in this ocean region opens up new insights for maritime safety.

Validation with altimeters wave data indicates that assimilating only wavenumbers components of partitions has a limited impact on reducing SWH bias and SI. The assimilation of SWH has obviously the largest contribution in reducing the SWH biases and SI. For instance, in the Arctic ocean region, the SWH bias is reduced by nearly 8 cm on average by either assimilating only SWH alone or by assimilating SWH and wavenumbers components. The Southern Ocean is an interesting ocean region where assimilating wavenumbers components seems to be as effective as assimilating only SWH in reducing bias and SI of SWH. As indicated by Aouf et al. (2021), in the Southern Ocean, where wind-wave growth faces unlimited fetch conditions, the assimilation of wavenumbers components of partitions is effective in compensating for uncertainties related to the nonlinear wave-wave interactions source terms in the wave model. This latter is represented in the wave model MFWAM through a DIA approximation.

The results of the comparison with the Spotter wave buoys in terms of bias and SI of SWH are consistent with those obtained with altimeters. Moreover, the comparison with buoys shows the substantial contribution of the assimilation of SWH in reducing SWH bias and SI, and the reduced impact of wavenumbers partitions assimilation in this respect, except for the Southern Ocean. In contrast, the assimilation of wavenumbers components of partitions efficiently reduces the bias and SI of peak period $T_p$. While the assimilation of SWH only yields to a degradation of the bias and SI of $T_p$ compared to control simulation without assimilation in North Atlantic and North Pacific regions. We also observed a slight degradation of bias of $T_p$ when the joint assimilation of SWH and wavenumbers components of partitions is activated, while SI of $T_p$ is significantly reduced. The only ocean region where the assimilation of SWH only has reduced the peak period bias is the Agulhas region. Indeed, in this region the sea state is dominated by swell regime (mean value of $T_p$ is about 12 s), which consistently supports the assumption of conservation of swell slope from Lionello et al. (1992) assimilation scheme. In order to keep this assumption valid, the difference of SWH induced by the assimilation of SWH necessarily leads to a change on $T_p$ of the same sign, and the correction on the bias of SWH induced by the assimilation of SWH also applies on the correction of $T_p$ bias. This conclusion also confirms the results in the Southern Ocean, which is mostly dominated by energetic long swell, as indicated in Aouf et al. (2021).

In other respects, the model performance in terms of statistical analysis evaluation compared to altimeters and wave buoys has been carried out during the forecast period. The improvements resulting from the assimilation of SWH and wavenumber components are particularly noticeable in the scatter index: the combined assimilation (SPEC_HS_ASSIM) induces the smallest scatter index of SWH and peak period compared to the other assimilation runs, and the impact remains persistent until 3 days in the forecast period. For the peak period bias, the assimilation of wavenumbers components of partitions (SPEC_ASSIM) has kept the smallest bias up to 5 days in the forecast. Regarding to long swells for peak period $T_p$ ranged between 12 and 18 s, all assimilation runs performed better the estimate of peak period than the control run during the forecast period, and the impact of combined assimilation (SPEC_HS_ASSIM) remains remarkably persistent until 7–10 days in the forecast. The study of the forecast period opens a room of improvement to have a better distribution of SWH correction induced by the assimilation on the frequency scale of the wave spectrum.

Several sources of uncertainty must be considered. First, the quality of SWIM data may vary across different ocean regions and wave regimes, as well as depending on the direction of wave propagation relative to along-track

satellite direction. Additionally, the drifting buoys network is relatively sparse outside ocean areas with strong currents. Another issue is the discrepancy in frequency intervals between buoy measurements and the model's spectral discretization, which can affect the accuracy of peak period calculations—a parameter particularly sensitive to spectral resolution methods.

Despite these technical challenges, there is potential for enhancing the assimilation scheme in the MFWAM model. The use of wave ensembles to characterize background model errors could be very helpful in order to improve the spread of optimal interpolation corrections. Further, the power laws given by Lionello et al. (1992) and Toledano et al. (2022), which has proven skillfulness in ocean regions with energetic, well-developed swells, could be adapted to better handle ocean areas dominated by less energetic wind seas or growing wind seas transitioning into swells. A possible improvement would be to assimilate the wind speed from SWIM to better estimate the empirical wind-wave growth laws involved in the assimilation scheme for wind-sea dominant ocean regions. Another suggestion can be the calibration of B coefficient in Equation 2 by using peak period from drifting wave buoys. This will give a more consistent estimate of the mean period compared to the buoys observations. We also can examine a simpler correction induced by the assimilation of SWH on the wave spectrum as described in Wang et al. (2024). However, this latter showed a very limited impact in wind-sea dominant ocean regions.

## Appendix A: Statistical Parameters

We define $N$ as the sample size, $Y_m$ as the model data and $Y_o$ as the observation data, and the statistical parameters as follows:

- The mean bias is defined as:

$$\text{Bias} = \frac{1}{N}\sum_{i=1}^{N}(Y_m - Y_o) \tag{A1}$$

- The scatter index is defined as:

$$\text{SI} = \frac{100 * \sigma(Y_m - Y_o)}{\text{mean}(Y_o)} \tag{A2}$$

where $\sigma$ is the standard deviation of the difference.

## Appendix B: Bias of IFS Wind Speed

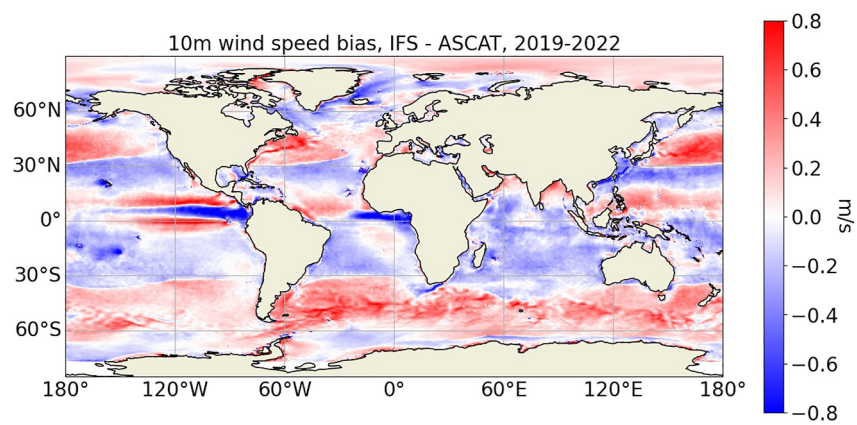


**Figure B1.** Global distribution of bias 10 m wind speed module of IFS-ECMWF model with ASCAT product, 2019–2022.

## Appendix C: Impact of the Assimilation in the Forecast Period for Extreme Values of $T_p$

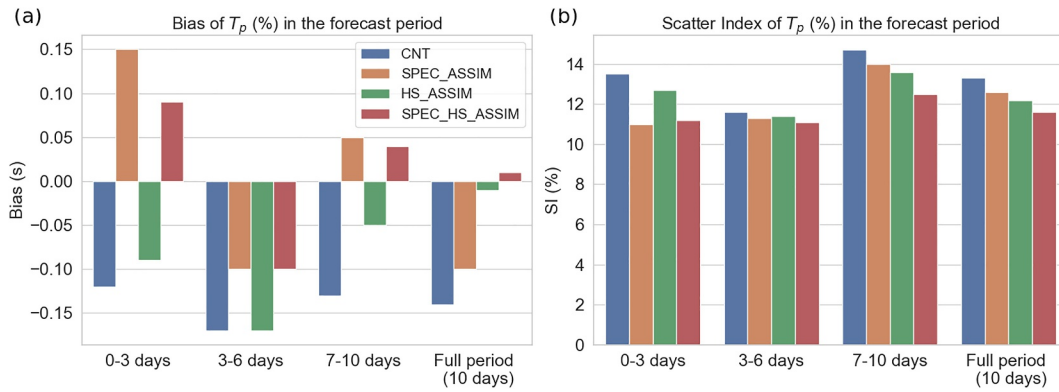


**Figure C1.** (a) $T_p$ bias and (b) SI of $T_p$ at different stages of the forecast period for $12 < T_p < 18$ s.

## Conflict of Interest

The authors declare no conflicts of interest relevant to this study.

## Availability Statement

CFOSAT/SWIM data are available on the AVISO web portal, after registration: https://www.aviso.altimetry.fr/fr/missions/missions-en-cours/cfosat/acces-aux-donnees.html. For validation, satellite data are available on Copernicus Marine Service https://data.marine.copernicus.eu/product/WAVE_GLO_PHY_SWH_L3_NRT_014_001/description, and SOFAR buoy data have been provided by Sofar Spotter Archive website https://www.sofarocean.com/mx/sofar-spotter-archive.

**Acknowledgments**
The authors acknowledge the CNES, the CNRM and Météo-France, who funded the thesis and research that led to this article. The authors also thank SOFAR Spotter for providing us with data from SOFAR Spotter buoys.

## References

Alday, M., & Ardhuin, F. (2023). On consistent parameterizations for both dominant wind-waves and spectral tail directionality. *Journal of Geophysical Research: Oceans*, *128*(4), e2022JC019581. https://doi.org/10.1029/2022JC019581

Aouf, L., Dalphinet, A., Hauser, D., Tison, C., Delaye, L., Chapron, B., et al. (2019). On the assimilation of CFOSAT wave data in the wave model MFWAM: Verification phase. In *IGARSS 2019—2019 IEEE international geoscience and remote sensing symposium, Yokohama, Japan, 2019* (pp. 7959–7961). https://doi.org/10.1109/IGARSS.2019.8900180

Aouf, L., Hauser, D., Chapron, B., Toffoli, A., Tourain, C., & Peureux, C. (2021). New directional wave satellite observations: Towards improved wave forecasts and climate description in Southern Ocean. *Geophysical Research Letters*, *48*(5), e2020GL091187. https://doi.org/10.1029/2020GL091187

Aouf, L., Lefèvre, J., & Hauser, D. (2006). Assimilation of directional wave spectra in the wave model WAM: An impact study from synthetic observations in preparation for the SWIMSAT satellite Mission. *Journal of Atmospheric and Oceanic Technology*, *23*(3), 448–463. https://doi.org/10.1175/JTECH1861.1

Aouf, L., & Lefèvre, J. M. (2015). On the impact of the assimilation of SARAL/AltiKa wave data in the operational wave model MFWAM. *Marine Geodesy*, *38*(sup1), 381–395. https://doi.org/10.1080/01490419.2014.1001050

Ardhuin, F., Erick, R., Babanin, A. V., Filipot, J. F., Magne, R., Roland, A., et al. (2010). Semiempirical dissipation source functions for ocean waves. Part I: Definition, calibration, and validation. *Journal of Physical Oceanography*, *40*(9), 191741. https://doi.org/10.1175/2010JPO4324.1

Babanin, A. V., Young, I. R., Rogers, W., Smith, J. M., & Tolman, H. L. (2014). Observation-based dissipation and input terms for spectral wave models, with end-user testing. https://doi.org/10.21236/ada616445

GCOS. (2016). The global observing system for climate: Implementation needs, GCOS-200. Retrieved from https://library.wmo.int/opac/doc_num.php?explnum_id=3417

Gerling, T. W. (1992). Partitioning sequences and arrays of directional ocean wave spectra into component wave systems. *Journal of Atmospheric and Oceanic Technology*, *9*(4), 444–458. https://doi.org/10.1175/1520-0426(1992)009<0444:PSAAOD>2.0.CO;2

Hanley, K. E., Belcher, S. E., & Sullivan, P. P. (2010). A global climatology of wind–wave interaction. *Journal of Physical Oceanography*, *40*(6), 1263–1282. https://doi.org/10.1175/2010JPO4377.1

Hasselmann, S., & Hasselmann, K. (1985). Computations and parameterizations of the nonlinear energy transfer in a gravity-wave spectrum. Part I: A new method for efficient computations of the exact nonlinear transfer integral. *Journal of Physical Oceanography*, *15*(11), 1369–1377. https://doi.org/10.1175/1520-0485(1985)015<1369:CAPOTN>2.0.CO;2

Hasselmann, S., Lionello, P., & Hasselmann, K. (1997). An optimal interpolation scheme for the assimilation of spectral wave data. *Journal of Geophysical Research*, *102*(C7), 15823–15836. https://doi.org/10.1029/96JC03453

Hauser, D., Tison, C., Amiot, T., Delaye, L., Corcoral, N., & Castillan, P. (2017). SWIM: The first spaceborne wave scatterometer. *IEEE Transactions on Geoscience and Remote Sensing*, *55*(5), 3000–3014. https://doi.org/10.1109/TGRS.2017.2658672

Hauser, D., Tourain, C., Hermozo, L., Alraddawi, D., Aouf, L., Chapron, B., et al. (2021). New observations from the SWIM radar on-board CFOSAT: Instrument validation and ocean wave measurement assessment. *IEEE Transactions on Geoscience and Remote Sensing*, *59*(1), 5–26. https://doi.org/10.1109/TGRS.2020.2994372

Houghton, I. A., Hegermiller, C., Teicheira, C., & Smit, P. B. (2022). Operational assimilation of spectral wave data from the Sofar Spotter network. *Geophysical Research Letters*, *49*(15), e2022GL098973. https://doi.org/10.1029/2022GL098973

Janssen, P., Aouf, L., Behrens, A., Korres, G., Cavalieri, L., Christiensen, K., & Breivik, Ø. (2014). Final report of work-package I, in 'My wave' project. Retrieved from http://repositorio.aemet.es/bitstream/20.500.11765/7249/3/MyWave_Report_D64.pd

Janssen, P., & Bidlot, J. (2023). Wind–Wave interaction for strong winds. *Journal of Physical Oceanography*, *53*(3), 779–804. https://doi.org/10.1175/JPO-D-21-0293.1

Kalnay, E. (2002). *Atmospheric modeling, data assimilation and predictability*. Cambridge University Press. https://doi.org/10.1017/CBO9780511802270

Lionello, P., Günther, H., & Janssen, P. A. E. M. (1992). Assimilation of altimeter data in a global third-generation wave model. *Journal of Geophysical Research*, *97*(C9), 14453–14474. https://doi.org/10.1029/92JC01055

Lionello, P., & Janssen, P. A. E. M. (1990). Assimilation of altimeter measurements to update swell spectra in wave models. In *Proc. of the international symposium on assimilation of observations in meteorology and oceanography (Clermont-Ferrand, France)* (pp. 241–246). World Meteorological Organization.

Rabault, J., Takehiko, N., Hope, G., Müller, M., Breivik, Ø., Voermans, J., et al. (2021). OpenMetBuoy-v2021: An easy-to-build, affordable, customizable, open-source instrument for oceanographic measurements of drift and waves in sea ice and the open ocean. *Geosciences*, *12*(3). https://doi.org/10.3390/geosciences12030110

Raghukumar, K., Chang, G., Spada, F., Jones, C., Janssen, T., & Gans, A. (2019). Performance characteristics of "Spotter," a newly developed real-time wave measurement buoy. *Journal of Atmospheric and Oceanic Technology*, *36*(6), 1127–1141. https://doi.org/10.1175/JTECH-D-18-0151.1

Saulter, A. N., Bunney, C., King, R. R., & Waters, J. (2020). An application of NEMOVAR for regional wave model data assimilation. *Frontiers in Marine Science*, *7*, 579834. https://doi.org/10.3389/fmars.2020.579834

Semedo, A., Sušelj, K., Rutgersson, A., & Sterl, A. (2011). A global view on the wind sea and swell climate and variability from ERA-40. *Journal of Climate*, *24*(5), 1461–1479. https://doi.org/10.1175/2010JCLI3718.1

Shimura, T., & Nobuhito, M. (2019). High-resolution wave climate hindcast around Japan and its spectral representation. *Coastal Engineering*, *151*, 19. https://doi.org/10.1016/j.coastaleng.2019.04.013

Smit, P. B., Houghton, I. A., Jordanova, K., Portwood, T., Shapiro, E., Clark, D., et al. (2021). Assimilation of significant wave height from distributed ocean wave sensors. *Ocean Modelling*, *159*, 101738. https://doi.org/10.1016/j.ocemod.2020.101738

Thomson, J., Lund, B., Hargrove, J., Smith, M. M., Horstmann, J., & MacKinnon, J. A. (2021). Wave-driven flow along a compact marginal ice zone. *Geophysical Research Letters*, *48*(3), e2020GL090735. https://doi.org/10.1029/2020GL090735

Timmermans, B. W., Gommenginger, C. P., Dodet, G., & Bidlot, J.-R. (2020). Global wave height trends and variability from new multimission satellite altimeter products, reanalyses, and wave buoys. *Geophysical Research Letters*, *47*(9), e2019GL086880. https://doi.org/10.1029/2019GL086880

Toledano, C., Ghantous, M., Lorente, P., Dalphinet, A., Aouf, L., & Sotillo, M. G. (2022). Impacts of an altimetric wave data assimilation scheme and currents-wave coupling in an operational wave system: The New Copernicus Marine IBI Wave Forecast Service. *Journal of Marine Science and Engineering*, *10*(4), 457. https://doi.org/10.3390/jmse10040457

Wang, C., Songlin, L., Huaming, Y., Kejian, W., Shuyan, L., & Ying, X. (2024). Comparison of wave spectrum assimilation and significant wave height assimilation based on Chinese-French oceanography satellite observations. *Remote Sensing of Environment*, *305*(2024), 114085. https://doi.org/10.1016/j.rse.2024.114085

Yu, H., Li, J., Wu, K., Wang, Z., Yu, H., Zhang, S., et al. (2018). A global high-resolution ocean wave model improved by assimilating the satellite altimeter significant wave height. *International Journal of Applied Earth Observation and Geoinformation*, *70*, 43–50. https://doi.org/10.1016/j.jag.2018.03.012

Zieger, S., Babanin, A. V., Rogers, W. E., & Young, I. R. (2015). Observation-based source terms in the third-generation wave model WAVEWATCH. *Ocean Modelling*, *96*, 225. https://doi.org/10.1016/j.ocemod.2015.07.014